This paper has been published in *Journal of Petrology* volume 45, number 8 (August 2004), pages 1631-1662.

Ultramafic xenoliths from the Bearpaw Mountains, Montana, USA: Evidence for multiple metasomatic events in the lithospheric mantle beneath the Wyoming craton

HILARY DOWNES[1], RAY MACDONALD[2], BRIAN G.J. UPTON[3], KEITH G. COX[4], JEAN-LOUIS BODINIER[5], PAUL R.D. MASON[6], DODIE JAMES[3], PETER G. HILL[3] and B CARTER HEARN JR[7]

[1] SCHOOL OF EARTH SCIENCES, BIRKBECK, UNIVERSITY OF LONDON, MALET STREET, LONDON WC1E 7HX, UK
[2] ENVIRONMENTAL SCIENCE DEPARTMENT, LANCASTER UNIVERSITY, LANCASTER LA1 4YQ, UK
[3] DEPARTMENT OF GEOLOGY AND GEOPHYSICS, UNIVERSITY OF EDINBURGH, WEST MAINS ROAD, EDINBURGH EH9 3JW, UK
[4] DEPARTMENT OF EARTH SCIENCES, UNIVERSITY OF OXFORD, OXFORD OX1 3PR, UK (deceased)
[5] ISTEEM, LABORATOIRE DE TECTONOPHYSIQUE, UMR 5568, CNRS ET UNIVERSITE DE MONTPELLIER 2, 34095 MONTPELLIER, CEDEX 02, FRANCE
[6] FACULTY OF GEOLOGY, UNIVERSITY OF UTRECHT, BUDAPESTLAAN 4, UTRECHT, THE NETHERLANDS
[7] US GEOLOGICAL SURVEY, NATIONAL CENTRE, RESTON, VIRGINIA 20192 USA

ABSTRACT

Ultramafic xenoliths in Eocene minettes of the Bearpaw Mountains volcanic field (Montana, USA), derived from the lower lithosphere of the Wyoming craton, can be divided based on textural criteria into tectonite and cumulate groups. The tectonites consist of strongly depleted spinel lherzolites, harzburgites and dunites. Although their mineralogical compositions are generally similar to those of spinel peridotites in off-craton settings, some contain pyroxenes and spinels that have unusually low Al_2O_3 contents more akin to those found cratonic spinel peridotites. Furthermore, the tectonite peridotites have whole-rock major element compositions that tend to be significantly more depleted than non-cratonic mantle spinel peridotites (high MgO, low CaO, Al_2O_3 and TiO_2) and resemble those of cratonic mantle. These compositions could have been generated by up to 30% partial melting of an undepleted mantle source.

Petrographic evidence suggests that the mantle beneath the Wyoming craton was re-enriched in three ways: (i) by silicate melts that formed mica websterite and clinopyroxenite veins; (ii) by growth of phlogopite from K-rich hydrous fluids; and (iii) by interaction with aqueous fluids to form orthopyroxene porphyroblasts and orthopyroxenite veins. In contrast to their depleted major element compositions, the tectonite peridotites are mostly LREE-enriched and show enrichment in fluid-mobile elements such as Cs, Rb, U and Pb on mantle-normalised diagrams. Lack of enrichment in high field strength elements (e.g. Nb, Ta, Zr and Hf) suggests that the tectonite peridotites have been metasomatised by a subduction-related fluid. Clinopyroxenes from the tectonite peridotites have distinct U-shaped REE patterns with strong LREE-enrichment. They have $^{143}Nd/^{144}Nd$ values that range from 0.5121 (close to the host minette values) to 0.5107, similar to those of xenoliths from the nearby Highwood Mountains. Foliated mica websterites also have low $^{143}Nd/^{144}Nd$ values (0.5113) and extremely high $^{87}Sr/^{86}Sr$ ratios in their constituent phlogopite,

indicating an ancient (probably mid-Proterozoic) enrichment. This enriched mantle lithosphere later contributed to the formation of the high-K Eocene host magmas.

The cumulate group ranges from clinopyroxene-rich mica peridotites (including abundant mica wehrlites) to mica clinopyroxenites. Most contain >30% phlogopite. Their mineral compositions are similar to those of phenocrysts in the host minettes. Their whole-rock compositions are generally poorer in MgO but richer in incompatible trace elements than those of the tectonite peridotites. Whole-rock trace element patterns are enriched in LILE (Rb, Cs, U and Pb) and depleted in HFSE (Nb, Ta Zr and Hf) as in the host minettes, and their Sr-Nd isotopic compositions are also identical to those of the minettes. Their clinopyroxenes are LREE-enriched and formed in equilibrium with a LREE-enriched melt closely resembling the minettes. The cumulates therefore represent a much younger magmatic event, related to crystallisation at mantle depths of minette magmas in Eocene times, that caused further metasomatic enrichment of the lithosphere.

KEY WORDS: ultramafic xenoliths; Montana; Wyoming craton; metasomatism; cumulates; minette

INTRODUCTION

Suites of ultramafic xenoliths from north-central USA provide an opportunity to assess the evolution of the mantle keel of the Wyoming craton. One of the greatest concentrations of such xenoliths is in the Bearpaw Mountains in Montana, where the host volcanism has been dated at 50-54 Ma (Marvin *et al*., 1980). The Bearpaw Mountains form part of an extensive Eocene high-K magmatic province (Fig. 1) that includes the Highwood Mountains (50-53 Ma), the Sweet Grass Hills (50-54 Ma), Eagle Buttes (50-52 Ma) and the Missouri Breaks diatremes (47-52 Ma) (Hearn, 1989a; O'Brien *et al*., 1991).

Aspects of the magmatism of the Bearpaw Mountains have been summarized by Hearn (1989 a, b) and Macdonald *et al*. (1992). The extrusive rocks are mainly latites and minettes. Ultramafic xenoliths are so abundant in the fragmental minette deposits that in some localities they compose up to 50% of the material. They range up to >1 m in diameter and vary from rounded to subrounded in shape. Samples investigated in this study include parts of xenoliths more than 1m in diameter, down to those that have dimensions in the 5-10 cm range. Contacts with the host minettes are sharp and there is no evidence of interaction between the host lava and the xenoliths. The relative proportions of xenolith types vary widely from locality to locality. Mica clinopyroxenites are present at all investigated sites and are often the most abundant ultramafic xenoliths. Only a few localities contain abundant olivine-rich or mica-free xenoliths. The percentage of composite or veined xenoliths is relatively small. Garnet peridotites are absent in the Bearpaw Mountains minettes but have been found in the Missouri Breaks kimberlite diatremes, about 70 km to the southeast (Hearn & McGee, 1984, 1987; McGee & Hearn, 1989; Carlson *et al*., 1999) and in the Porcupine Dome region of SE Montana (Hearn, 1999).

The ultramafic xenoliths discussed in this paper come from two localities: Little Sand Creek (47°57.9′N 109°32.1′W) and Warrick Creek (48°3.7′N 109°35.4′W). Mineral chemistry and whole-rock major and trace element analyses of the xenoliths, together with mineral trace element and isotopic data, are presented in order to: (1) document depletion and enrichment events in the mantle lithosphere of the Wyoming craton; (2) determine the origin of the ultramafic xenoliths (restites vs cumulates); (3) investigate the relationship between the ultramafic cumulates and their host minette magmas.

PETROGRAPHY

Ultramafic xenoliths of the Bearpaw Mountains include a wide range of lithologies from olivine-dominant to clinopyroxene- and/or mica-dominant (Table 1). They can be clearly divided

on the basis of macro- and micro- structures into two groups. One group (referred to here as the "tectonite suite") shows the typical deformation textures of mantle-derived spinel peridotites worldwide, including porphyroclastic and coarse granular textures. The tectonite suite is composed mainly of fresh to slightly serpentinised spinel harzburgites, with rarer spinel lherzolites, dunites and wehrlites. A distinct sub-group of the tectonite suite are harzburgites that contain white orthopyroxene porphyroblasts and veins. These latter xenoliths tend to be strongly altered to serpentine. Different types of veins cross-cut the tectonite peridotites: (1) foliated mica websterites; (2) mica clinopyroxenites grading to glimmerites; (3) white orthopyroxenites and (4) Cr-diopside clinopyroxenites.

The second group contains largely undeformed peridotites and pyroxenites with clearly cumulus textures, including interstitial and poikilitic mica ± clinopyroxene ± orthopyroxene. This is referred to as the "cumulate suite" and consists of micaceous lherzolites, dunites, harzburgites, wehrlites, and mica clinopyroxenites with or without olivine, grading to olivine-free glimmerites in which phlogopite content exceeds that of clinopyroxene. Photomicrographs showing the textures of the two suites are shown in Fig. 2.

The modal mineralogy of representative xenoliths is given in Table 1. Mineral proportions were determined from single thin-sections, counting between one thousand and two thousand points. However, given the textural variability in many of the rocks and the serpentinization that has affected some tectonite xenoliths, the modes are only approximate.

The analysed tectonite samples include a dunite LSC 247, five harzburgites, one lherzolite LSC 263, one wehrlite LSC 260, and two strongly altered harzburgites that contain white orthopyroxene in hand specimen (WC 296, WC 297). They vary texturally from coarse granular rocks, in which the olivines show strain lamellae, to strongly porphyroclastic with orthopyroxene showing exsolution lamellae of clinopyroxene. Foliated samples contain elongate porphyroclasts of olivine and orthopyroxene up to 1cm in length, holly-leaf spinels (Fig. 2a) and lenses of phlogopite-spinel aggregates. Phlogopite occurs as either disseminated grains or around Cr-spinel.

Many of the white-orthopyroxene harzburgites contain veins of orthopyroxenite up to 10 mm wide. Some contain multiple subparallel veins of white orthopyroxenite that are cross-cut at high angles by younger orthopyroxenite veins, suggesting a joint pattern that was exploited by the fluids from which the orthopyroxene crystallised. The veins locally contain up to 10% phlogopite or up to 20% olivine and trace amounts of spinel. Ragged porphyroblasts of orthopyroxene are also present in some of these samples (Fig. 2b). In this study, two white-orthopyroxenite harzburgites have been studied. Sample WC 296 is a highly tectonised spinel harzburgite, containing orthopyroxene porphyroclasts up to 1 cm in diameter. Sample WC 297 is also a harzburgite, containing olivine (largely serpentinised) and orthopyroxene with an average grain size around 2 mm, and small amounts (~2%) of spinel and phlogopite. Veins of orthopyroxene 1-3 mm wide cut both samples but have no discernible effect on the surrounding host. The white orthopyroxenes are often altered to a mixture of K-feldspar and mica.

Two foliated mica websterite samples (LSC 188, LSC 197) were also analysed. From their deformed nature, we regard them as part of the tectonite suite, but their origin may be as cumulates formed within veins cutting the tectonites. LSC 197 contains strongly oriented mica (29%) together with large orthopyroxene crystals (up to 6 mm across) which are dominant over clinopyroxene (Fig. 2 c, d). Rare crystals of zircon are also present. LSC 188 contains equidimensional clinopyroxene and subordinate orthopyroxene (6%), ilmenite (3.6%), abundant apatite, rare zircon and very rare monazite. Mica forms 36% of the rock and has a strong preferred orientation (Fig. 2 e).

The phlogopite-rich cumulate peridotite xenoliths differ significantly from the peridotite textonites in texture and modal mineralogy. Cumulate peridotites WC 253, WC 232 and WC 251 form a sub-group that is much richer in olivine than the other samples with interstitial (rather than poikilitic) phlogopite (Fig. 2f). Typically they contain idiomorphic olivine, up to 10 mm across,

with oikocrysts, up to 20 mm across, of phlogopite and colourless diopside and, in most cases, orthopyroxene (Fig. 2g). Phlogopite forms 12 -50% of these rocks. The textures strongly suggest that these rocks formed as cumulates. Spinel is present in only trace amounts, as small opaque grains that occur as clusters or enclosed in the silicates. Needles of apatite are also present, as is rare barite. The modal mineralogy of these rocks (Table 1) shows high clinopyroxene/ orthopyroxene ratios, so that most of the samples are wehrlites or clinopyroxene-rich lherzolites, although two samples that have extremely low pyroxene contents (WC 232; LSC 233) are mica dunites.

The mica-clinopyroxenite xenoliths range from olivine-bearing types in which clinopyroxene appears to have started crystallizing after olivine, to olivine-free varieties. There is a continuum from mica-rich clinopyroxenites to clinopyroxene-bearing glimmerites. The pyroxene-rich varieties have heteradcumulate textures, with euhedral olivines up to 4 mm, and smaller diopsides and spinels enclosed in pale brown phlogopite oikocrysts (Fig. 2h,i,j). Apatite ranges from stout prisms to slender needles, usually enclosed in phlogopite and is most abundant in glimmeritic veins. Glimmerite LSC 225 contains 80% randomly orientated interlocking phlogopite crystals, up to 4mm across, together with euhedral to subhedral clinopyroxene crystals (20%) up to 2mm in diameter.

MINERAL CHEMISTRY

Mineral analyses were performed at the Department of Geology and Geophysics, University of Edinburgh, on a Cambridge Scientific Instruments "Microscan 5" electron probe microanalyser, using the wavelength dispersive method. Pure elements, oxides and simple silicate compositions were used as standards. Corrections were made for dead-time, atomic number, absorption and fluorescence using computer programmes based on the methods of Sweatman & Long (1969). The operating conditions were 20 kV and a sample current of 30 nA. A 30s counting interval was used for peaks; backgrounds were counted for 15s.

Olivine

Olivines in the tectonite peridotite xenoliths (Table 2) are unzoned and are the most highly magnesian, with CaO, MnO and NiO abundances similar to those in Type 1 ultramafic xenoliths (Frey & Prinz, 1978; Galer & O'Nions, 1989; Lee *et al.*, 1996). Their highest Fo values (91.8) are from the harzburgites and dunites. NiO concentrations vary from 0.42 wt. % to 0.34 wt. %, except for olivines in the harzburgites with white orthopyroxene, which have slightly lower abundances (0.28-0.34 wt. % NiO). Figure 3 shows a plot of mole % Fo against wt. % NiO content in which olivines from the tectonites fall in a single field. This field largely overlaps that of olivines in spinel peridotite xenoliths from non-cratonic areas worldwide (e.g., McDonough & Rudnick, 1998); however the Bearpaw olivines have slightly lower Fo contents than those found in cratonic mantle, for example from East Greenland (Bernstein et al., 1998), South Africa (Boyd et al., 1999) and Tanzania (Lee and Rudnick, 1999).

The cumulate mica peridotites contain olivines of Fo_{92-78} composition with NiO concentrations varying from 0.26 to 0.40 wt. %. Although some of these compositions overlap those in the tectonite peridotites, most have lower NiO and significantly lower Fo contents (Fig. 3). They can also be slightly zoned, with iron-rich rims. Olivines in the cumulate mica clinopyroxenites are Fo_{83-77} and their NiO contents are lower (0.23-0.26 wt. %) than olivine in the other xenolith types. In general, the olivine compositions in the cumulate xenoliths overlap those of the phenocrysts (and possibly xenocrysts) observed in the host minettes (Fig. 3).

Spinel

Spinel group minerals in the tectonite peridotites (Table 3) range from spinels with low Cr/(Cr+Al) and high $Mg/(Mg+Fe^{2+})$ to magnesiochromites found in dunite LSC 247 and wehrlite

LSC 260 (Fig. 4a). This trend is similar to that normally found in off-craton mantle peridotites worldwide (McDonough & Rudnick, 1998), although the two magnesiochromites have high Cr/(Cr+Al) values that resemble spinels found in cratonic mantle peridotites. Spinels in the cumulate mica peridotites and mica clinopyroxenites generally have compositions distinct from those in the tectonites (Fig. 4a), with higher Cr/(Cr+Al) ratios and variable Mg/(Mg+Fe^{2+}) ratios. However, their compositions overlap those of the magnesiochromites from the most depleted tectonites.

The relationship between the Fo content of olivine and Cr/(Cr+Al) in coexisting spinels (Fig. 4b) shows that, while the tectonite peridotite samples fall mostly within the depletion trend established for non-cratonic mantle peridotites worldwide (McDonough & Rudnick, 1988), some of them extend the trend to extremely depleted values similar to those of cratonic peridotites (e.g. Bernstein et al., 1998; Lee and Rudnick, 1999). The tectonite harzburgites with white orthopyroxene (WC 296, WC 297) fall below the global peridotite field, as their olivines have anomalously low Fo contents. Spinels in the cumulate mica peridotites tend to have higher Cr/(Cr+Al) ratios than most of the tectonite peridotites, and their coexisting olivines have slightly lower Fo contents (Fig. 4b). This trend is more extreme in the mica clinopyroxenites, which have olivine with very low Fo contents and spinels with high Cr/(Cr+Al) ratios. The mineral compositional variation thus supports the petrographic groupings of the xenoliths.

Orthopyroxene

Orthopyroxenes in most tectonite peridotites show little variation in composition (En_{92-91}). The white orthopyroxene from harzburgites WC 296 and WC 297 have slightly lower Mg# (En_{89}) (Table 4; Fig. 5a). The range in the cumulate mica peridotites is En_{92-87}, whereas orthopyroxene in the foliated mica websterites is much more iron-rich (En_{77-63}). Enstatite values are positively correlated with the Fo content of coexisting olivines.

All orthopyroxenes in Bearpaw xenoliths are Al-poor (< 3 wt. % Al_2O_3). However, those in sample WC 297, a tectonite harzburgite with white orthopyroxene, are extremely Al-poor (Al_2O_3 < 1 wt. %) and have highly variable Al_2O_3 contents. Orthopyroxenes with < 2 wt. % Al_2O_3 are unusual in spinel peridotite xenoliths in non-cratonic environments (Lee *et al*., 1996; Witt-Eickschen & Kramm, 1997; Luhr & Aranda-Gomez, 1997). However, cratonic spinel peridotites (e.g. from Greenland, South Africa and Tanzania) tend to have lower Al_2O_3 contents (Fig. 5a). Nevertheless, the white orthopyroxenes from the Bearpaw harzburgite xenoliths are among the most Al-deficient yet recorded from spinel peridotites, similar to those reported by Smith and Riter (1997) from Arizona and by Rudnick et al. (1994) from Olmani, Tanzania. The rare orthopyroxenes in the cumulate mica peridotites are also Al-poor, but those in the mica websterites have more normal Al_2O_3 contents (Fig. 5a).

Clinopyroxene

Whilst all clinopyroxenes in the tectonite peridotites and cumulate mica peridotites are diopsides, those in the cumulate xenoliths are slightly more Fe-rich (Table 5). Cr_2O_3 concentrations are generally < 1 wt. %. Clinopyroxenes in the cumulate mica clinopyroxenites range from diopside to salite. *Mg*-numbers vary from 0.94 in the peridotites to 0.44 in the clinopyroxenites and correlate positively with *mg*-numbers of olivine and orthopyroxene. The mica websterites show similarly low *mg*-numbers (40-46). Like the orthopyroxenes, the clinopyroxenes tend to be Al-poor and there is a general positive correlation between the Al_2O_3 contents of orthopyroxenes and clinopyroxenes (Tables 4 and 5). Clinopyroxenes in the tectonite lherzolites plot towards the Al-poor end of the global mantle peridotite field of McDonough & Rudnick (1998) (Fig. 5b) and more closely resemble clinopyroxenes from cratonic spinel peridotites. There is a general increase in Al, Ti, Mn and Na, and decrease in Cr from the cumulate mica peridotites to the mica clinopyroxenites, as the

mg-numbers of the clinopyroxenes decrease. Clinopyroxenes from the cumulate xenoliths tend to fall within the field of phenocryst clinopyroxenes from the host minettes (Fig. 5b).

Micas

Mg-numbers of phlogopites vary from 0.95 to 0.92 in the tectonite peridotites and from 0.93 to 0.83 in cumulate mica peridotites (Table 6). The mica clinopyroxenites have lower Mg-numbers (0.82-0.78) but those in the mica websterites have much more variable values (0.73 –0.89). There is a good correlation between *mg*-numbers of the phlogopites and those of the coexisting olivines and pyroxenes. Figure 6 shows that, with one exception (LSC 238), there is separation between the compositions of micas in the clinopyroxenites and those in the peridotites. The micas are not notably Ti-rich, generally containing < 2.3 wt. % TiO_2. Phlogopites from the peridotites (both tectonite and cumulate types) fall in the field of mantle phlogopites. Those in the clinopyroxenites tend to have higher TiO_2 contents and overlap the field of phlogopite phenocrysts in the host minettes (Fig. 6). Al_2O_3 content ranges from 12.2 to 16.4 wt. % and does not correlate with lithology (Table 6).

Geothermometry and oxygen barometry

Because of the absence of orthopyroxene and/or clinopyroxene from some samples, only the olivine-spinel geothermometer of Ballhaus *et al*. (1991) was applicable to all the olivine-bearing samples (Table 7). Both the tectonites and cumulates yield similar temperature ranges (tectonites = 830-1090°C; cumulates = 930-1010°C). Oxygen fugacity values have been calculated using the oxygen barometer of Ballhaus *et al*. (1991), using temperatures calculated by their method and an assumed equilibration pressure of 20 kbar. Fe^{2+} and Fe^{3+} values in spinel were calculated from electron microprobe analyses assuming stoichiometry. $\Delta(fO_2)^{FMQ}$ values in the tectonite peridotites range from –1.1 to +1.2, i.e. close to the FMQ buffer, similar to other subcontinental peridotite xenoliths (Ionov & Wood, 1992; Canil *et al*., 1994; Alibert, 1994; Qi *et al*., 1995; Wiechert *et al*., 1997). The cumulate mica peridotites are slightly more oxidised ($\Delta(fO_2)^{FMQ}$ + 0.3 to + 1.1), possibly due to higher water pressure, as indicated by the presence of abundant phlogopite.

WHOLE ROCK GEOCHEMISTRY

XRF whole-rock analyses were made using a Philips PW1480 spectrometer at the University of Edinburgh, calibrated using CRPG and USGS reference standards (Govindaraju, 1994). Major elements were determined on fused glass discs (Norrish & Hutton, 1969) and trace elements were determined on pressed powder pellets. A full description of the techniques used, analytical conditions and precision estimates is given in Fitton *et al*. (1998). Results are given in Tables 8-10. Since the xenoliths show variable values of Loss on Ignition, the major element data have been recalculated on an anhydrous basis before being plotted on chemical variation diagrams.

Although abundances of many trace elements in the Bearpaw xenolith suite are close to the detection limits of the XRF technique, elements such as Cr, Ni, Zr, Ba, Rb, Sr, V, Sc and Zn are above detection limit in most samples (Tables 8-10). Further trace element determinations (including full REE data) were made using ICP-MS at the University of Montpellier using a VG-PQ2 spectrometer (Table 11). Powders were dissolved in a $HClO_4$-HF mixture in closed beakers on a hot-plate for 24 hours. This procedure was repeated using smaller amounts of acids for a further 12 hours. A small amount of $HClO_4$was added and evaporated three times, followed by a final dissolution in HNO_3 and dilution for analysis. REE, U, Th, Sr, Zr, Hf, Rb and Ba concentrations were measured by external calibration, following the procedure described by Ionov *et al*. (1992). Nb and Ta concentrations were calibrated using Zr as an internal standard. Godard *et al*. (2000) have evaluated the precision of Montpellier ICP-MS analyses at low concentration levels from

repeated analyses of the international standard PCC-1. The precision is in the range 1-5% for most elements, except for Sm, Gd and Hf (5-6%), and Eu (about 9%). Accuracy of the ICP-MS analyses can be evaluated from the analysis of international standard UB-N analysed during this study (Table 11). Agreement between XRF and ICP-MS results is excellent for Rb and Sr, whereas there is a slight discrepancy in Ba, with the XRF value tending to be higher than the ICP-MS value at high concentrations. However, while the agreement between the two methods for Zr is excellent for most samples, the two mica websterites yielded much higher Zr contents by XRF than by ICP-MS (e.g. 89 ppm vs 36 ppm). This may reflect a problem with a small quantity of undissolved zircons and may also affect the ICP-MS result for Hf in these two samples.

Major element variations

The tectonite peridotites have higher MgO contents and a smaller range (42-49 wt. % MgO) than normally found in off-craton spinel peridotite xenoliths but almost perfectly overlap the range of spinel peridotites from cratonic regions (Fig. 7). Al_2O_3, CaO and TiO_2 contents are also very low and again overlap the field of cratonic spinel peridotite whole-rock compositions. Thus the compositions vary between moderately and extremely depleted relative to average spinel peridotite subcontinental lithosphere (McDonough, 1990). As would be expected from their depleted mineralogy, dunites and harzburgites tend to have lower SiO_2, TiO_2, Al_2O_3 and CaO contents than the lherzolites (Table 8). The white-orthopyroxene harzburgites are compositionally similar to the other tectonite peridotites, apart from having higher Fe_2O_3 contents, in keeping with their more Fe-rich mineral phases. The major element data suggest that compositional variation in the tectonite xenoliths is mainly attributable to differing degrees of melting of fertile mantle source rocks, but that the white-orthopyroxene harzburgites have experienced an additional process which has raised their iron content.

The cumulate mica peridotites show a wide range of MgO contents (anhydrous) from 44 to 25 wt. % (Fig. 7). With three exceptions, there is a complete separation in terms of MgO content between the rocks with tectonised textures and those with cumulate textures. The exceptions are three cumulate samples, mica wehrlite WC 253 and mica dunites WC 232 and WC 251, all of which have > 41 wt. % MgO (Table 8). These have significantly less phlogopite and more olivine than the other cumulate mica peridotites, and the phlogopite is interstitial rather than poikilitic (Table 1). Their whole-rock compositions thus reflect their high olivine contents. The least magnesian cumulate mica peridotites have higher TiO_2, Al_2O_3 and CaO contents and overlap in composition with the cumulate mica clinopyroxenites. The range reflects not only an increased abundance of phlogopite and clinopyroxene at the expense of olivine and orthopyroxene and also changes in mineral composition. The foliated mica websterites tend to have even lower MgO contents and much more variable concentrations of TiO_2, Al_2O_3 and CaO, probably reflecting mineralogical control (e.g. websterite LSC 197 is rich in orthopyroxene, whereas LSC 188 is clinopyroxene-rich).

K_2O contents of the tectonite peridotites vary from < 0.05 wt. % up to 0.2 wt. % in one of the white-opx harzburgites (Fig. 7), probably reflecting the traces of phlogopite in this rock. Some overlap with the low values shown by cratonic spinel peridotites, whereas other have higher values typical of non-cratonic spinel peridotites. K_2O contents in the cumulate mica-bearing xenoliths are very high (> 1.8wt. %), reflecting the abundance of phlogopite, with glimmerite LSC 225 having the highest value (~7 wt. %). Na_2O values are below detection limit for the tectonite xenoliths and the olivine-rich cumulate mica peridotites. In the remaining cumulate mica peridotites and pyroxenites Na_2O values are uniform (0.39-0.75 wt. %), similar to those in the mica websterites. P_2O_5 values range from low (< 0.05 wt. %) in the tectonite peridotites to high values (> 0.6 wt. %) in the cumulate mica clinopyroxenites, reflecting the greater abundance of apatite in the latter.

Trace element variations (XRF)

Figure 8 shows the variation of selected compatible (Ni, Cr) and incompatible (Rb, Sr) trace elements in the Bearpaws xenoliths, plotted against MgO. Ni concentrations in the tectonite peridotites are similar to (or slightly lower than) those of off-craton spinel peridotite xenoliths (insufficient data are available for spinel peridotites from cratonic areas for a meaningful field to be plotted). Concentrations of Ni in the cumulate suite decrease with decreasing MgO contents, due to the lower amount of modal olivine. Three samples plot above the general trend: cumulate mica wehrlite LSC 220 and two foliated mica websterites LSC 188 and LSC 197. Cr contents in the tectonite peridotites are at the lower end of the field for spinel peridotites, except for dunite LSC 247 that has an extremely high Cr content (4260 ppm). This is presumably related to the fact that LSC 247 has the highest spinel content among the tectonites (3.2 %) and the spinel is extremely Cr-rich (62 wt. % Cr_2O_3).

Rb contents are lowest in the tectonite peridotites but, as would be expected from their mica-rich lithologies, they are high in the cumulate peridotites and clinopyroxenites (18-150 ppm) and exceptionally high (337 ppm) in glimmerite LSC 225 (Fig. 8). Sr concentrations in most of the tectonite peridotites are generally low, typical of mantle spinel peridotites, except in wehrlite LSC260 in which the high Sr content (105 ppm) reflects the high modal proportion of clinopyroxene. The cumulate xenoliths all have high Sr contents (> 150 ppm), with the exception of the three olivine-rich samples that plot in the tectonite field (Fig. 8). Since clinopyroxene and apatite are the main hosts for Sr, the Sr content is dictated by the amount of these two minerals in the rock. The absolute abundance of apatite in the xenoliths is hard to determine, but the cumulate xenoliths with highest Sr contents appear to contain moderate amounts of cumulus apatite. Ba contents are variable, those in the tectonite peridotites being generally < 70 ppm, increasing to 150-2070 ppm in the cumulate mica peridotites and 1650-2600 ppm in the cumulate mica pyroxenites and glimmerite. This relates to the amount of phlogopite in the rock, as the phlogopites contain up to 1.0 wt% BaO (Table 6). In contrast, the foliated mica websterites have lower Ba values (480-780 ppm), reflecting the low BaO content of their constituent micas (0.23-0.28 wt. %). Zr contents likewise vary with lithology. Those from the tectonite peridotites are low (<13 ppm) whereas those from the cumulate xenoliths are distinctly higher (5-22 ppm, with the lowest value from a mica dunite). The two foliated mica websterites have high but very variable Zr contents, reflecting their mineralogy (clinopyroxene-rich sample LSC 188 has 89 ppm Zr, compared with orthopyroxene-rich sample LSC 197 with 31 ppm Zr).

Trace element variations (ICP-MS)

The majority of the tectonite peridotites are LREE-enriched with $(La/Yb)_n$ from 5.1 to 12.0, with no significant Eu anomalies (Table 11; Fig. 9). Some show slightly U-shaped REE patterns, indicative of strong depletion overprinted by LREE-enrichment. The mantle-normalised whole-rock trace element patterns of the tectonite peridotites (Fig. 10) show overall LILE enrichment, with particularly strong peaks in the fluid-mobile elements Cs, U and Pb, and commonly have significant troughs at the high field strength elements Nb-Ta and Zr-Hf. However, the two harzburgites with white orthopyroxene (WC 296, WC 297) have flatter REE patterns ($(La/Yb)_n$ = 1.1 – 7.8) with significant negative Eu anomalies (Eu/Eu* = 0.53-0.57), indicating a different origin for these samples.

The two foliated mica websterites exhibit contrasting whole-rock trace element and REE patterns, presumably reflecting their different clinopyroxene/ orthopyroxene ratios. In general the clinopyroxene-rich sample LSC 188 has a much higher concentration of incompatible trace elements than the orthopyroxene-rich sample LSC 197. Both have negative Eu anomalies (Fig. 9), but the REE pattern for LSC 197 is much flatter than that of LSC 188. $(La/Yb)_n$ is 1.3 in LSC 197 (orthopyroxene-rich) and 8 in LSC 188 (clinopyroxene-rich). Both have high concentrations of Cs,

Rb, Ba and Pb, reflecting their high phlogopite contents (Fig. 10). Troughs at Hf for these two samples may be artifacts caused by incomplete dissolution of zircon.

The cumulate mica clinopyroxenites and the glimmerite (LSC 225) have very uniform whole-rock REE compositions (Fig. 9) with $(La/Yb)_n$ values ranging from 7.1 to 12.6. The cumulate mica peridotites have nearly identical REE patterns ($(La/Yb)_n$ = 5.7 – 12.0) and completely overlap the patterns of the mica clinopyroxenites. On a mantle-normalised diagram (Fig. 10) the cumulate mica peridotites and mica clinopyroxenites show extremely similar trace element patterns, strongly suggesting that the two rock-types are closely related and were probably precipitated from the same type of magma. They are strongly enriched in LILE (Cs, Rb, Ba, U and Pb) and depleted in HFSE (Nb, Ta, Zr and Hf). This reflects both their mineralogy (dominated by phlogopite and clinopyroxene) and the nature of the magma from which they were formed. The trace element patterns of the whole-rock mica clinopyroxenites closely resemble those of high-K minettes from the Bearpaw Mountains (Macdonald *et al*., 1992), with high LILE (particularly Pb) and low HFSE (Fig. 10). Thus it is very probable that these cumulates were formed from magma closely related to the host minettes.

Rb/Sr ratios in the tectonite peridotites are unusually high, varying from 0.03 to 1.4, with the highest values in the two harzburgites with white orthopyroxene. Those of the cumulate mica peridotites and pyroxenites are less variable (0.32 – 1.02), although glimmerite LSC225 has a very high value (2.38), in accord with its mineralogy. The two foliated mica websterites also have extremely high Rb/Sr values (1.6 and 4.3), reflecting their high proportions of phlogopite and variable amounts of clinopyroxene.

TRACE ELEMENT SIGNATURES IN CLINOPYROXENES

Clinopyroxenes from five selected xenoliths were mounted in epoxy resin and analysed for trace elements at the University of Utrecht, using a 193 nm GeoLas (MicroLas) laser ablation system and a Platform ICP (Micromass) ICPMS. Ablation produced a crater 120 μm in diameter and approximately 100 μm deep. The laser shot repetition rate was 10 Hz and the laser power density was 10 J cm^{-2}. Data were collected using time-resolved software and processed using the technique of Longerich *et al*. (1996). Calibration was performed against the NIST612 standard glass, using the values of Pearce *et al*. (1997). ^{43}Ca, previously measured by electron microprobe, was used as an internal standard. Data for a mantle clinopyroxene RP91-17 (Mason *et al*., 1999) analysed at the same time agree with previously determined values to within 10%. External precision was ± 5% for concentrations > 1 ppm. Full REE and a selection of other incompatible trace elements were analysed (Table 12).

Clinopyroxenes from tectonite wehrlite LSC 260 are strongly zoned with respect to their trace elements, with cores abnormally rich in Ba and Rb (Table 12). However, even the rim of clinopyroxene from LSC 260 is much richer in these elements than the other clinopyroxenes, probably as the result of the presence of phlogopite inclusions within the crystal. The identification of phlogopite is also suggested by the lack of a significant difference in the REE elements between the two shot points. Cumulate mica wehrlite LSC 201 shows similar trace element zoning in its clinopyroxenes.

Figure 11 presents chondrite-normalised REE data for clinopyroxenes from the Bearpaws ultramafic xenoliths; trace element abundances normalised to primitive mantle are shown in Fig. 12. The two tectonite samples (lherzolite LSC 263 and wehrlite LSC 260) have clinopyroxenes with very similar REE patterns, showing extremely low HREE contents (< 5x chondritic). This probably indicates an original harzburgitic paragenesis, since extensive melting removes HREE from the mantle. The REE patterns are U-shaped with a minimum at Dy and strong LREE-enrichment ($(La/Yb)_n$ = 14.8-11.94). They have strong negative anomalies in Zr and Hf (Fig. 12), with that in lherzolite LSC263 being extreme (Zr and Hf being < 0.1 x primitive mantle values). As seen in xenoliths from elsewhere in the world, such anomalies are thought to result from extensive

melting of the lithospheric mantle followed by strong enrichment in LILE and LREE (Downes, 2001; Downes et al., 2003).

The REE patterns for clinopyroxene from cumulate xenoliths such as mica wehrlite LSC201 and mica clinopyroxenite LSC 237 differ from those for the tectonite clinopyroxenes. Whilst LREE-enriched ($(La/Yb)_n$ = 2.3-2.8), they show depletion in La and Ce relative to Nd and Sm (Fig. 11) and depletion in Zr and Hf relative to Nd and Sm (Fig. 12). The REE pattern of a melt in equilibrium with these two cumulates would have had a LREE-enriched pattern, very similar to that of the host minettes (Fig. 11).

The REE pattern for clinopyroxene from foliated mica websterite LSC 188 is also LREE-enriched ($(La/Yb)_n$ = 7.4) but with a slight negative Eu anomaly. In the mantle-normalised diagram (Fig. 12) it shows a strong negative Sr anomaly that might indicate that the clinopyroxene crystallised from a magma from which a Sr-rich phase (not necessarily plagioclase) had also separated. Judging from their occurrence as veins in the tectonite peridotites, the foliated mica websterites may be cumulates precipitated within dyke-like conduits. They were clearly formed from a different magma than the cumulate mica peridotites and clinopyroxenites.

Comparison with whole-rock compositions

Figure 13 shows a comparison of the LA-ICP-MS incompatible trace element data for clinopyroxenes from the Bearpaw xenoliths with the whole-rock analyses of the same samples. For the two tectonite xenoliths (LSC 260, LSC 263), the whole-rock patterns have a broadly similar shape as those of the constituent clinopyroxene, but at 8-10 x lower concentrations. This indicates that clinopyroxene is the main carrier of these trace elements in the tectonite peridotites. In sample LSC 263, the Zr, Hf, Rb and Ba contents of the whole rock are slightly higher than those of the clinopyroxene, suggesting a different host for these elements. In both samples U is much greater in the whole-rock than in the clinopyroxenes.

The comparison between clinopyroxene and whole-rock analyses for the mica websterite LSC 188 and the mica cumulates LSC 237 and LSC 201, however, shows a very different picture. The whole rock values are nearly identical to those of the constituent clinopyroxene for the REE and Zr, Hf, Sr and Y (Fig. 13). This is presumably a result of the large concentration of clinopyroxene in these samples (35-55 modal %, see Table 1) contributing to the whole-rock composition. On the other hand, the Rb, Ba, Th, U, Ta and Nb concentrations in the whole-rocks are much higher than those in the constituent clinopyroxenes. These trace elements must therefore be sequestered in the other minerals in these samples, i.e. phlogopite (Rb, Ba), apatite (U, Th), or on grain-boundary phases (Nb, Ta).

Sr AND Nd ISOTOPES

Clinopyroxenes from five of the xenoliths were separated by hand-picking under a binocular microscope. In some cases, it was not possible to ensure that inclusions of other minerals such as phlogopite were excluded. It was particularly difficult to separate pure clinopyroxene from the foliated mica websterite sample LSC 188, but fairly pure "books" of phlogopite could be readily separated from this sample (see below). The Sr and Nd isotope compositions of the clinopyroxenes were analysed at the University of London Radiogenic Isotope Laboratory (Table 12). Approximately 0.1 g of the separated pyroxenes was leached in hot 6M HCl for 2 hours. The rinsed samples were dissolved in HF and HNO_3, then taken up in 6M HCl. Sr and Nd were separated by conventional exchange columns. Sr was loaded onto single Ta filaments and Nd onto single Re filaments and run as an oxide. A VG354 multicollector mass spectrometer fitted with five collectors was used to analyse $^{87}Sr/^{86}Sr$ and $^{143}Nd/^{144}Nd$. Standard SRM987 gave an average $^{87}Sr/^{86}Sr$ value of 0.710239 ± 10 and an internal "Aldrich" standard yielded an average $^{143}Nd/^{144}Nd$ value of 0.511414 ± 4, equivalent to a value of 0.511857 for the La Jolla international standard (Thirlwall, 1991).

Data were obtained for clinopyroxenes from two tectonites (lherzolite LSC 263 and wehrlite LSC 260), a cumulate mica peridotite (LSC 201), a cumulate mica clinopyroxenite (LSC 237) and a foliated mica websterite (LSC 188). The isotope results have not been corrected to the age of eruption of the host minettes, as the Rb and Sr contents of the dissolved samples were not determined. An approximate age correction can be made from the Rb and Sr contents determined by LA-ICPMS but, as these vary greatly between shot-points in some of the clinopyroxenes, such Rb/Sr ratios are very approximate.

Present-day Sr and Nd isotope ratios for clinopyroxenes from the Bearpaws xenoliths fall in the enriched field of the Sr-Nd diagram (Fig. 14). Thus they are very different from the spinel peridotite xenoliths entrained from beneath regions of young (Phanerozoic) crust (e.g., Downes, 2001). The data fall essentially into two groups: those which have isotope ratios similar to those of the host minettes (cumulate mica wehrlite LSC 201, cumulate mica clinopyroxenite LSC 237 and tectonite wehrlite LSC 260) and those that plot away from isotopic composition of the hosts. Samples that plot in the field of the host minettes have either crystallised from magmas similar to the hosts, or were subject to extremely strong interaction with minette magma either before or during entrainment. This seems to be the most likely case for tectonite wehrlite LSC 260, which has an extremely unusual modal mineralogy for a mantle peridotite (Table 1).

The other xenoliths (tectonite lherzolite LSC 263 and foliated mica websterite LSC 188) have much lower $^{143}Nd/^{144}Nd$ values of 0.51074 – 0.51126 than the host minettes. Carlson & Irving (1994) reported similarly low $^{143}Nd/^{144}Nd$ values for mantle xenoliths from the nearby Highwood Mountains. In the case of tectonite lherzolite LSC 263, this may result from the time-integrated effects of its low Sm/Nd ratio (0.125) during long residence in the lithospheric mantle. Mica websterite LSC188 has an extremely high $^{87}Sr/^{86}Sr$ ratio (0.74844 ± 1) which almost certainly results from contamination of the clinopyroxene separate by high Rb/Sr mica, as it was extremely difficult to separate pure clinopyroxene from this sample. However, the Rb/Sr value for the clinopyroxene analysed by LA-ICPMS is low (0.02) and age correction to 52 Ma has very little effect on the $^{87}Sr/^{86}Sr$ ratio. Using the whole-rock Rb/Sr ratio (1.7) also has little effect.

Model ages

Isotopic data for Bearpaws ultramafic xenoliths provide some evidence on the timing of depletion in the mantle of the Wyoming craton. A major depletion event in the lithospheric mantle between 2.9 and 2.5 Ga is indicated by Re depletion model ages for peridotite xenoliths from the Highwood Montains and Eagle Buttes (Carlson & Irving, 1994), whereas xenoliths from the Missouri Breaks diatremes gave Re model ages of 1.7-2.5 Ga (Carlson *et al.*, 1999). Harzburgite and glimmerite xenoliths from the Highwood Mountains also yielded late Archaean Nd model ages (Carlson & Irving, 1994), whereas peridotites from Eagle Buttes give slightly younger model ages (2.4 - 1.6 Ga). In the Bearpaw suite, the T_{DM} (Nd) model age for tectonite lherzolite LSC 263 is 2.45 Ga, whereas a much younger age (1.13 Ga) is given by tectonite wehrlite LSC 260. The latter may represent a mixed age, between that of the original mantle depletion event and a later LREE-enrichment event, particularly as the $^{143}Nd/^{144}Nd$ value of this sample is very close to that of the host minettes.

Phlogopite was separated from foliated mica websterite LSC 188, its Sr isotope ratio was determined, and its Rb and Sr contents were analysed by isotope dilution (Table 12). From these data a Sr-isotope model age can be calculated, assuming a present-day undepleted mantle value of 0.7045 and an $^{87}Rb/^{86}Sr$ ratio of 0.0816. This calculation yields an age of around 1.25 Ga, suggesting a Proterozoic age for formation of the phlogopite in this sample. Glimmerite veins in xenoliths from the Highwood Mountains yield zircon and monazite ages around 1.8 Ga (Rudnick *et al*., 1993; Carlson & Irving, 1994), strongly suggesting that the mantle beneath the Wyoming craton underwent metasomatism involving the growth of phlogopite sometime in the mid-Proterozoic.

DISCUSSION

Petrographically, the Bearpaws xenoliths fall into several groups (Table 1). The most significant differences are related to the degree of deformation. Spinel peridotite tectonites have been strongly deformed and mica websterites show strong mineral foliations. Mica from a foliated websterite yields a mid-Proterozoic age and thus the deformation must post-date this time. In contrast, the micaceous cumulate xenoliths have pristine undeformed textures and therefore must be younger than the deformation event(s). Thus, phlogopite must have been introduced into the mantle beneath the Wyoming craton on at least two separate occasions, i.e. before and after deformation. The first enrichment was probably related to the formation of the glimmerites at 1.8 Ga (Rudnick *et al*., 1999) and foliated mica websterites (ca.1.2 Ga). The second enrichment event probably took place during the late Mesozoic or early Tertiary. Here we assess the nature of the early mantle depletion and the subsequent metasomatic events in the light of the new data from the Bearpaw xenolith suite.

Depletion in Bearpaw tectonite peridotites

Depletion by partial melting was extensive in the mantle represented by the Bearpaw tectonite peridotites. They have very low Al_2O_3 contents in both whole-rocks and mineral phases, comparable to cratonic mantle spinel peridotites from elsewhere in the world. To estimate the proportion of melt removed from the tectonite peridotites, we have followed the simple major element mass balance calculation method used by Bernstein *et al*. (1998). The average composition of the tectonite dunite and harzburgites was subtracted from the hypothetical primitive upper mantle composition of Hart & Zindler (1986) to give a melt composition in equilibrium with the average olivine composition in the xenoliths (Fo_{92}), using an olivine/liquid Fe/Mg Kd at 2.5 GPa of 0.365 (Ulmer, 1989). The estimated degree of melting is 28%. This value is consistent with the results of melting experiments (Walter, 1998), where residues of melting at 3 GPa reached $Fo_{91\text{-}92}$ at melt fractions between 17 and 30%.

Clinopyroxene occurs only in trace amounts in the tectonite harzburgites (Table 1), suggesting that parts of the mantle reached clinopyroxene-out during partial melting. This is consistent with experimental evidence; in primitive peridotites, clinopyroxene is consumed at *c*. 20-30% melting in the pressure range 1.5-4.0 GPa (Hirose & Kushiro, 1993; Takahashi *et al*., 1993; Walter, 1998). The anomalous abundance of clinopyroxene in the tectonite wehrlite LSC 260 may, in contrast, be a result of metasomatism, as the Sr-Nd isotope composition of these clinopyroxenes is very similar to that of the host minettes (Table 12; Fig. 14).

The trace element concentrations of the constituent clinopyroxenes can also be used to calculate the amount of melt removed from a primitive mantle protolith, based on the method of Norman (1998). To produce the low Y and Yb contents in clinopyroxenes in the tectonite samples LSC 260 and LSC 263 requires 15-18% melt extraction, assuming fractional melting of a mantle source containing 16% clinopyroxene. However, both samples actually plot above the theoretical melting trend. This calculation assumes that the clinopyroxenes are primary but this is almost certainly not the case in tectonite wehrlite LSC 260, whose modal composition is so unusual. The lack of agreement with the theoretical melting trend is a further indication that the tectonite xenoliths have experienced later metasomatism.

Multiple metasomatic events in the lithosphere of the Wyoming craton

The Bearpaw xenolith suite provides evidence for the introduction of several types of material into the depleted mantle: (i) dyke-like bodies of mica websterite, (ii) mica clinopyroxenite and mica peridotite cumulates, (iii) phlogopite ± apatite ± zircon, either in disseminated form or as glimmerite veins, and (iv) white orthopyroxene, as veinlets or porphyroblasts. Of these, only the mica websterites are strongly foliated. Several other features indicate that the mica websterites are

not cogenetic with the micaceous cumulate suite. The mantle-normalised trace element patterns of whole rocks and clinopyroxenes show significant differences from those of the cumulate mica clinopyroxenites, most notably in having a Sr trough, a negative Eu anomaly, and only a minor trough at Zr (Fig. 12). Carlson & Irving (1994) suggested that glimmerite veins in harzburgites beneath the Highwood Mountains represent the crystallization products, in mid-Proterozoic times, of migrating fluids and/or melts. Glimmerite veins in a harzburgite from the same locality yield zircon and monazite ages around 1.8 Ga (Rudnick *et al*., 1993; Carlson & Irving, 1994), which may have implications for the age of phlogopite metasomatism in the mantle beneath the Bearpaw Mountains. Phlogopite analysed from foliated mica websterite LSC 188 in this study also requires considerable time (ca 1.2 Ga) to evolve to its high $^{87}Sr/^{86}Sr$ ratio. The nature of the mid-Proterozoic mantle processes that led to the metasomatism remains unknown.

The undeformed nature of the rare phlogopite present in some tectonite peridotites indicates that it was introduced, recrystallized or redistributed after tectonism but before incorporation of the xenoliths into the host magmas. Phlogopite introduction presumably occurred, therefore, within the early Tertiary. The tectonite peridotites have K/Rb ratios in the range 97-173, notably lower than the ratio of 394 in the primitive mantle (Sun & McDonough, 1989). Rb/Sr ratios, in contrast, are often higher in the tectonites (0.05-1.8) than in the primitive mantle (0.03). Clinopyroxenes in tectonite peridotites LSC 263 and LSC 260 have Zr/Nd ratios of 0.02 and 0.92 (Table 12), whereas the ratio in primitive mantle is 8.3. The metasomatising agent in the mantle beneath the region was thus able to transport Rb relative to K, Rb relative to Sr, and LREE relative to HFSE, and therefore was probably a hydrous fluid (Tatsumi *et al*., 1986; Keppler, 1996; You *et al*., 1996).

Mica peridotite and clinopyroxenite xenoliths lacking metamorphic textures are also common in the Highwood Mountains and Eagle Buttes and have been interpreted by O'Brien *et al*. (1991) as crystallization products of the minette magmas. In the cumulate xenolith suite of the Bearpaw Mountains, there is a continuum from mica peridotite xenoliths to mica clinopyroxenites in which diopsidic pyroxene appears as the second cumulus phase after olivine, and from these into mica clinopyroxenites in which olivine is subordinate or absent (Table 1). The inferred crystallization sequence, olivine + spinel -> clinopyroxene -> phlogopite, with indications of a reaction relationship involving growth of phlogopite at the expense of olivine in both the cumulate xenoliths and the minettes (Macdonald *et al.*, 1992), suggests that the xenoliths are cognate to the minettes. Furthermore, the mineral chemistry of the cumulate xenoliths bears close overall similarities to that of the phenocryst assemblages in the minettes (Figs. 3-6). Whole-rock trace element patterns for the mica peridotite and clinopyroxenite cumulates (Fig. 10) are virtually identical to those of the minettes. The calculated REE patterns of melts in equilibrium with the constituent clinopyroxenes from these xenoliths are very similar to those of the minettes (Fig. 11). The cognate relationship between the cumulate xenoliths and the minettes is strongly supported by the similarity of the Sr and Nd isotopic data for the two groups (Fig. 14). We infer, therefore, that the undeformed mica peridotite cumulates are products of crystallization of minette magmas during early Tertiary times.

Using the xenolith data alone, we have no constraints on the pressures at which the mica clinopyroxenites formed. However, comparison of compositions of the phases in the xenoliths with those of the phenocrysts in the minettes suggests that the clinopyroxenites crystallized from melts with mg-number between 75 and 60. Macdonald *et al*. (1992) suggested, from comparison with experimental data, that minettes in this range of *mg*-numbers crystallised at pressures around 1.5 GPa. Whilst this estimate is poorly constrained, it may indicate that the cumulates formed at deep crustal or uppermost mantle levels.

Origin of white orthopyroxenes

Evidence bearing on the origin of the white orthopyroxenite veins and orthopyroxene porphyroblasts is as follows: (1) the orthopyroxenes tend to have even lower Al_2O_3 contents than

those in the host peridotites; (2) minerals within tectonite xenoliths that contain white orthopyroxenes tend to be more Fe-rich than those in other tectonite peridotites; (3) the orthopyroxenite veins had relatively little chemical or mineralogical effect on their host peridotites. Hearn *et al*. (1991) suggested that the low Al_2O_3 contents of orthopyroxenes may indicate that the protoliths were garnet peridotites, displaced into the spinel stability field. However, this cannot explain their existence in several generations of cross-cutting veins.

Smith and Riter (1997) discussed the origin of orthopyroxene porphyroblasts in mantle xenoliths from Arizona and concluded that they formed from hydration of the mantle, via the formation of and dehydration of chlorite peridotite. In this context, it may be significant that the samples containing white orthopyroxene (WC 296, WC 297) are extremely altered and contain highly serpentinised olivine. The low-Al nature of the white orthopyroxenes may indicate that they formed from a fluid that could not carry aluminium. We favour an origin by reaction of the tectonite peridotites with aqueous fluids that may have been related to, but perhaps had lower K/H_2O than, the K-rich fluids responsible for phlogopite growth. Aqueous fluids experimentally equilibrated with peridotite at 1.5 GPa and 750°C contain about 3 wt% solute rich in Si and poor in Mg (Schneider & Eggler, 1986). Migration of such fluids into the tectonites may well have resulted in reaction of olivine to form orthopyroxene. Alibert (1994) proposed this mechanism for the origin of enstatite megacrysts in peridotite xenoliths from the Colorado Plateau. She suggested that the fluids had been released from the subducted Farallon oceanic plate. O'Brien *et al*. (1991; 1995) and Carlson & Irving (1994) have presented evidence for a mantle metasomatised by fluids, perhaps from the Farallon plate, in the potassic rocks of the Wyoming Province. McInnes (1996) also ascribed the formation of orthopyroxene veins in peridotites from Papua New Guinea to infiltration by hydrous fluid. Kesson and Ringwood (1989) also suggested that interaction with subduction-zone fluids may cause an increase in orthopyroxene in the mantle above a Benioff zone. However, none of these suggestions seem to explain the unusual features of the whole-rock REE patterns of the white-orthopyroxene peridotites, which have prominent negative Eu anomalies (Fig. 9).

The timing of the proposed hydration event beneath the Bearpaw Mountains is not well constrained but it must have occurred when at least some of the mantle tectonites were cold enough to be jointed, given the evidence that the veins in some rocks followed a joint pattern. The fluids responsible for the orthopyroxenite veins might have been released from crystallizing minette magmas at greater depth or from decomposition of phlogopite into garnet + Al-poor phlogopite + relatively siliceous fluid (Sato *et al*., 1997). The presence of low-Al orthopyroxene in the cumulate mica peridotites (Table 4, Fig. 5a) indicates that the event that formed these minerals may have been related to the minette magmatism, despite the lack of orthopyroxene on the liquidus of minettes.

Origin of high-K magmatism

The origin of the Eocene high-K province and related alkaline magmatism in Wyoming and Montana has been investigated by numerous authors (e.g. Fraser *et al*., 1985; Dudas *et al*., 1987; Meen & Eggler, 1987; Eggler *et al.*, 1987; Mitchell *et al*., 1987; Scambos & Farmer, 1988; Hyndman *et al*., 1988; Irving, 1990; O'Brien *et al*., 1991, 1995; Dudas, 1991; Macdonald *et al*., 1992). Most authors agree that at least three mantle components are required in their petrogenesis, one of which is probably ancient enriched lithospheric mantle with low $^{143}Nd/^{144}Nd$ values. The tectonite peridotites and mica websterites described in this paper probably represent this enriched component. They have $^{143}Nd/^{144}Nd$ values (0.5107-0.5113) and variable $^{87}Sr/^{86}Sr$, depending on the proportion of phlogopite present. Magmas from Smoky Butte and Leucite Hills (Fraser *et al*., 1985; Vollmer *et al.*, 1984) require a source with low $^{87}Sr/^{86}Sr$ values similar to those of tectonite peridotite LSC 263, whereas those from the Highwood Mountains (O'Brien *et al*., 1991) require higher $^{87}Sr/^{86}Sr$ values in their source, e.g. a mixture between LSC 263 and mica websterite LSC

188. A further mantle component is an asthenospheric source, represented by the compositions of kimberlites from the Missouri Breaks area (Macdonald *et al*., 1992).

O'Brien *et al*. (1991, 1995) invoked subduction processes for the formation of the Eocene high-K magmas in central Montana. They suggested that the potassic magmas could have been generated by decompression melting within a mica-bearing mantle wedge that had been metasomatised during Cretaceous times by fluids derived from the subducting Farallon plate. These melts then underwent interaction with ancient, phlogopite-rich, metasomatic veins within the keel of the Wyoming Craton. In contrast, we suggest that the effect of Cretaceous subduction was to produce water-rich fluids that formed the white orthopyroxene veins and the disseminated phlogopite in the spinel peridotite tectonites. The water-souble trace elements may have also enriched the convecting asthenospheric mantle wedge above the Farallon plate, forming the asthenospheric end-member for the magmatism. The minette magmas generated in the Wyoming Craton lithosphere underwent crystallisation in deep magma chambers, producing the cumulate mica peridotites and clinopyroxenites. Some of the minettes also reacted with the ancient mantle lithosphere, forming wehrlites such as sample LSC 260.

Mica peridotite and clinopyroxenite xenoliths lacking metamorphic textures are common in the high-K magmatic province of Wyoming and Montana and have been interpreted in this paper and by O'Brien *et al*. (1991) as crystallization products of minette magmas. From comparison with experimental data for the pseudo-quaternary system olivine-augite-sanidine-kalsilite, Macdonald *et al.* (1992) suggested that the primary magmas of the Bearpaw minettes could have been generated by partial melting of an olivine + clinopyroxene + phlogopite- bearing mantle at pressures somewhat lower than 3 GPa. This is broadly consistent with the idea that the primary melts were generated within the spinel peridotite facies, close to the spinel - garnet transition zone.

CONCLUSIONS

The ultramafic xenoliths from the Bearpaw Mountains can be divided into (i) tectonite and (ii) mica-rich cumulate suites. Compositional variations in the tectonite peridotites are related to depletion by up to 30% melting, followed by metasomatic overprinting events firstly in Proterozoic times and then shortly prior to Eocene magmatism. The tectonites are veined by mica websterites and mica clinopyroxenites, which are interpreted as crystallization products from melts. Foliated mica websterites occurring in veins in the tectonite xenoliths differ sufficiently in mineralogy and geochemistry from the cumulate suite for them to be considered as products of a separate (and much older) metasomatic event. A later metasomatism has resulted from an influx of hydrous fluids, which resulted in growth of orthopyroxenite veins and porphyroblasts, together with some mica in the tectonite suite.

The cumulate suite comprises clinopyroxene-rich mica peridotites and mica clinopyroxenites. They have chemical and isotopic signatures very similar to those of the Eocene minette magmas, as well as having mineral compositions similar to those of the phenocrysts in the minettes. Thus they are inferred to be the crystallization products of Eocene minette magmas. The minette magmas are derived from a complex source including lithospheric components represented by the tectonite peridotites and foliated mica websterites described in this paper.

ACKNOWLEDGEMENTS

The late Keith Cox was an inspirational colleague and friend for many years. We sadly miss his insights, innovativeness and humour. We thank K.D. Collerson and D.B. Stewart for help in the field, and Andy Beard for help with the photomicrographs and back-scatter identification of accessory phases. Stefan Bernstein, Rick Carlson and Marge Wilson provided very helpful comments on earlier versions of the manuscript. The detailed contribution of Roberta Rudnick to the final version is gratefully acknowledged. RM acknowledges tenure of a Visiting Fellowship at All Souls College, Oxford, during the initial preparation of this paper. The Radiogenic Isotope

Laboratory at Royal Holloway was formerly a University of London Intercollegiate Research Facility. This project was funded by N.A.T.O.

REFERENCES

Alibert, C. (1994). Peridotite xenoliths from western Grand Canyon and The Thumb: A probe into the subcontinental mantle of the Colorado Plateau. *Journal of Geophysical Research* **99**, 21605-21620.

Ballhaus, C., Berry, R.F. & Green, D.H. (1991). High pressure experimental calibration of the olivine-orthopyroxene-spinel oxygen geobarometer: implications for the oxidation state of the upper mantle. *Contributions to Mineralogy and Petrology* **107**, 27-40.

Bernstein, S., Kelemen, P.B. & Brooks, C.K. (1998). Depleted spinel harzburgite xenoliths in Tertiary dykes from East Greenland: Restites from high degree melting. *Earth and Planetary Science Letters* **154**, 221-235.

Canil, D., O'Neill, H.St.C., Pearson, D.G., Rudnick, R.L., McDonough, W.F. & Carswell, D.A. (1994). Ferric iron in peridotites and mantle oxidation states. *Earth and Planetary Science Letters* **123**, 205-220.

Carlson, R.W. & Irving, A.J. (1994). Depletion and enrichment history of subcontinental lithospheric mantle: An Os, Sr, Nd and Pb isotopic study of ultramafic xenoliths from the northwestern Wyoming Craton. *Earth and Planetary Science Letters* **126**, 457-472.

Carlson, R.W., Irving, A.J. & Hearn, Jr., B.C. (1999). Chemical and isotopic systematics of peridotite xenoliths from the Williams kimberlite, Montana: clues to processes of lithosphere formation, modification and destruction. *Proceedings of the VIIth International Kimberlite Conference*, vol 1, 90-98.

Downes, H. (2001). Formation and modification of the shallow sub-continental lithospheric mantle; a review of geochemical evidence from ultramafic xenolith suites and tectonically emplaced ultramafic massifs of western and central Europe. *Journal of Petrology* **42**, 233-250.

Downes H, Reichow M, Mason P R D, Beard A D & Thirlwall M F. (2003). Mantle domains in the lithosphere beneath the French Massif Central: trace element and isotopic evidence from mantle clinopyroxenes. *Chemical Geology* **200**, 71-87.

Dudas, F.O. (1991). Geochemistry of igneous rocks of the Crazy Mountains, Montana, and tectonic models for the Montana alkalic province. *Journal of Geophysical Research* **96**, 13261-13277.

Dudas, F.O., Carlson, R.W. & Eggler, D.H. (1987). Regional Middle Proterozoic enrichment of the subcontinental mantle source of igneous rocks from central Montana. *Geology* **15**, 22-25.

Eggler, D.H., McCallum, M.E. & Kirkley, M.B. (1987). Kimberlite-transported nodules from Colorado-Wyoming; a record of enrichment of shallow portions of an infertile lithosphere. *Geological Society of America, Special Paper* **215**, 77-90.

Fitton, J.G., Saunders, A.D., Larsen, L.M., Hardason, B.S. & Norry, M.J. (1998). Volcanic rocks from the southeast Greenland margin at 63°N: composition, petrogenesis and mantle sources. In: Saunders, A.D., Larsen, H.C. & Wise, S.H.(eds) *Proceedings of the ODP Scientific Results* **152**. Texas: College Station, pp. 331-350.

Fraser, K.J., Hawkesworth, C.J., Erlank, A.J., Mitchell, R.H. & Scott-Smith,B.H. (1985). Sr, Nd, and Pb isotope and minor-element geochemistry of lamproites and kimberlites. *Earth and Planetary Science Letters* **76**, 57-70.

Frey, F.A. and Prinz, M. (1978). Ultramafic inclusions from San Carlos, Arizona; petrologic and geochemical data bearing on their petrogenesis. *Earth and Planetary Science Letters* **34**, 129-176.

Galer, S.J.G. & O'Nions, R.K. (1989). Chemical and isotopic studies of ultramafic inclusions from the San Carlos Volcanic Field, Arizona: a bearing on their petrogenesis. *Journal of Petrology* **30**, 1033-1064.

Godard, M., Jousselin, D. & Bodinier, J.-L., 2000. Relationships between geochemistry and structure beneath a palaeo-spreading centre: A study of the mantle section in the Oman ophiolite *Earth and Planetary Science Letters* 180, 133-148.

Govindaraju, K. (1994). 1994 compilation of working values and sample description for 383 geostandards. *Geostandards Newsletter* **18**, 1-158.

Guo, J. & Green, T.H. (1990). Experimental study of barium partitioning between phlogopite and silicate liquid at upper-mantle pressure and temperature. *Lithos* **24**, 83-95.

Hart, S.R. & Zindler, A. (1986). In search of a bulk-earth composition. *Chemical Geology* **57**, 247-267.

Hearn, Jr., B.C. (1989a). Introduction - T346 Montana high-potassium igneous province. In : *Montana High-Potassium Igneous Province. Field Trip Guidebook T346*. Washington, DC: American Geophysical Union, pp. 1-5.

Hearn, Jr., B.C. (1989b). Bearpaw Mountains, Montana. In : *Montana High-Potassium Igneous Province; Field Trip Guidebook T346*. Washington, DC: American Geophysical Union, pp. 51-61.

Hearn, Jr., B.C. & McGee, E.S. (1984). Garnet peridotites from Williams kimberlites, north-central Montana, U.S.A. In: Kornprobst, J. (ed.) *Kimberlites II: The Mantle and Crust-Mantle Relationships*. Amsterdam: Elsevier, pp. 57-70.

Hearn, Jr., B.C. & McGee, E.S. (1987). Crust and upper mantle beneath the northern plains; evidence from xenoliths. *U.S. Geological Survey, Circular* **956**, 32-34.

Hearn, Jr., B.C., Collerson, K.D., Upton, B.G.J. & Macdonald, R. (1991). Ancient and enriched upper mantle beneath north-central Montana: evidence from xenoliths. *Montana Bureau of Mines and Geology Special Publication* **100**, 133-135.

Hearn, Jr., B.C (1999). Peridotite xenoliths from Porcupine Dome, Montana, USA: depleted subcontinental lithosphere samples in an olivine-phlogopite-carbonate magma. *Proceedings of the VIIth International Kimberlite Conference*, vol. 1, 353-360.

Hirose, K. & Kushiro, I. (1993). Partial melting of dry peridotites at high pressures: Determination of compositions of melts segregated from peridotites using aggregates of diamond. *Earth and Planetary Science Letters* **114**, 477-489.

Hyndman, D.W., Tureck-Schwartz, K. & Foland, K.A. (1988). Chemical and isotopic evidence for potassic mafic magmas from an old K-enriched mantle source and for Eocene crustal melting in the central Montana alkalic province. *Geological Society of America Abstracts with Programs* **20**, A195.

Ionov, D.A. & Wood, B.J. (1992). The oxidation state of subcontinental mantle: oxygen thermobarometry of mantle xenoliths from central Asia. *Contributions to Mineralogy and Petrology* **111**, 179-193.

Ionov D A, Savoyant L and Dupuy C 1992. Application of the ICP-MS technique to trace-element analysis of peridotites and their minerals. Geostand. Newsletter 16, 311-315.

Irving, A.J. (1990). Montana Archean lithospheric mantle: chemical constraints from Eu-anomalous ultramafic xenoliths in minette. *EOS, Transactions of the American Geophysical Union* **71**, 1712.

Keppler, H. (1996). Constraints from partitioning experiments on the composition of subduction-zone fluids. *Nature* **380**, 237-240.

Kohler, T.P. & Brey, G. (1990). Calcium exchange between olivine and clinopyroxene calibrated as a geothermobarometer for natural peridotites from 2 to 60 kb with applications. *Geochimica et Cosmochimica Acta* **54**, 2375-2399.

Leake. B.E. and 21 others (1997). Nomenclature of amphiboles; report of the subcommittee on amphiboles of the International Mineralogical Association commission on new minerals and mineral names. *Mineralogical Magazine* **61**, 295-321.

Lee, D.-C., Halliday, A.N., Davies, G.R., Essene, E.J., Fitton, J.G. & Temdjim, R. (1996). Melt enrichment of shallow depleted mantle: a detailed petrological, trace element and isotopic study of mantle-derived xenoliths and megacrysts from the Cameroon Line. *Journal of Petrology* **37**, 415-441.

Lee, C.-T. and Rudnick, R. L. (1999). Compositionally stratified cratonic lithosphere: petrology and geochemistry of peridotite xenoliths from the Labait volcano, Tanzania. Preoc. VIIth Internat. Kimb. Conf. 503-521.

Longerich, H.P., Jackson, S.E. & Gunther, D. (1996). Laser ablation inductively coupled plasma – mass spectrometric transient signal data acquisition and analyte concentration calculation. *Journal of Analytical Atomic Spectrometry* **11**,899-904.

Luhr, J.F. & Aranda-Gomez, L.J. (1997). Mexican peridotite xenoliths and tectonic terranes: correlations among vent location, texture, temperature, pressure, and oxygen fugacity. *Journal of Petrology* **38**, 1075-1112.

Macdonald, R., Upton, B.G.J., Collerson, K.D., Hearn, Jr., B.C. and James, D. (1992) Potassic mafic lavas of the Bearpaw Mountains, Montana: mineralogy, chemistry, and origin. *Journal of Petrology* **33**, 305-346.

Marvin, R.F., Hearn, B.C., Jr., Mehnert, H.H., Naeser, C.W., Zartman, R.E. & Lindsey, D.A. (1980). Late Cretaceous-Paleocene-Eocene igneous activity in north-central Montana. *Isochron/West* **29**, 5-25.

Mason, P.R.D., Jarvis, K.E., Downes, H. & Vannucci, R. (1999). Determination of incompatible trace elements in mantle clinopyroxenes by LA-ICP-MS: a comparison of analytical performance with established techniques. *Geostandards Newsletter: The Journal of Geostandards and Geoanalysis* **23**, 157-172.

McDonough, W.F. (1990). Constraints on the composition of the continental lithospheric mantle. *Earth and Planetary Science Letters* **101**, 1-18.

McDonough, W.F. & Rudnick, R.L. (1998). Mineralogy and composition of the upper mantle. In: Hemley, R.J. (ed.) *Ultrahigh-Pressure Mineralogy: Physics and Chemistry of the Earth's Deep Interior. Reviews in Mineralogy* **37**. Washington D.C. : Mineralogical Society of America, 139-164.

McGee, E.S. & Hearn, Jr., B.C. (1989). Primary and secondary mineralogy of carbonated peridotites from the MacDougal Springs diatreme. In: O'Reilly, S.Y., Ferguson, J. & Janse, A.J.A. (eds) *Kimberlites and Related Rocks. Geological Society of Australia Special Publication* **14**, 725-734.

McGregor, I.D. (1974). The system MgO-Al_2O_3-SiO_2: solubility of Al_2O_3 in enstatite for spinel and garnet peridotite compositions. *American Mineralogist* **59**, 110-119.

McInnes, B (1996). Fluid-peridotite interactions in mantle wedge xenoliths. *EOS Transactions of the American Geophysical Union* **77**, S282.

Meen, J.K. & Eggler, D.H. (1987). Petrology and geochemistry of the Cretaceous Independence volcanic suite, Absoroka Mountains, Montana: clues to the composition of the Archean sub-Montana mantle. *Geological Society of America Bulletin* **98**, 238-247.

Mitchell, R.H. (1986). *Kimberlites: Mineralogy, Geochemistry and Petrology*. New York: Plenum, 442 pp.

Mitchell, R.H., Platt, R.G. & Downey, M. (1987). Petrology of lamproites from Smoky Butte, Montana. *Journal of Petrology* **28**, 645-677.

Mueller, P.A. & Wooden, J.L. (1988). Evidence for Archean subduction and crustal recycling, Wyoming Province. *Geology* **16**, 871-874.

Nicolas, A., Lucazeau, F. & Bayer, R. (1987). Peridotite xenoliths in Massif Central basalts, France: textural and geophysical evidence for asthenospheric diapirism. In: Nixon, P.H. (ed.) *Mantle Xenoliths*. London: Wiley & Sons, pp. 563-574.

Norman, M.D. (1998). Melting and metasomatism in the continental lithosphere: Laser ablation ICPMS analysis of minerals in spinel lherzolites from eastern Australia. *Contributions to Mineralogy and Petrology* **130**, 240-255.

Norrish, K. & Hutton, J.T. (1969). An accurate spectrographic method for the analysis of a wide range of geological samples. *Geochimica et Cosmochimica Acta* **33**, 431-453.

O'Brien, H.E., Irving, A.J. & McCallum, I.W. (1991). Eocene potassic magmatism in the Highwood Mountains, Montana: petrology, geochemistry and tectonic implications. *Journal of Geophysical Research* **96**, 13237-13260.

O'Brien, H.E., Irving, A.J., McCallum, I.S. & Thirlwall, M.F. (1995). Strontium, neodymium, and lead isotopic evidence for the interaction of post-subduction asthenospheric potassic mafic magmas of the Highwood Mountains, Montana, USA, with ancient Wyoming craton lithospheric mantle. *Geochimica et Cosmochimica Acta* **59**, 4539-4556.

O'Reilly, S.Y., Chen, D., Griffin, W.L. and Ryan, C.G. (1997). Minor elements in olivine from spinel lherzolite xenoliths: implications for thermobarometry. *Mineralogical Magazine* **61**, 257-269.

Pearce, N.J.G., Perkins, W.T., Westgate, J.A., Gorton, M.P., Jackson, S.E., Neal, C.R. & Chenery, S.P. (1997). A compilation of new and published major and trace element data for NIST SRM 610 and NIST SRM 612 glass reference materials. *Geostandards Newsletter: The Journal of Geostandards and Geoanalysis* **21**, 115-144.

Qi, Q., Taylor, L.A. & Zhou, X. (1995). Petrology and geochemistry of mantle peridotite xenoliths from SE China. *Journal of Petrology* **36**, 55-75.

Rudnick, R.L., McDonough W F and Orpin A., 1994. Northern Tanzanian peridotite xenoliths: a comparison with Kaapvaal peridotites and inferences on metasomatic interactions. *Proceedings of the VIIth International Kimberlite Conference*, 336-353.

Rudnick, R.L., Ireland, T.R., Gehrels, G., Irving, A.J., Chesley, J. T. & Hanchar, J. M., 1999. Dating mantle metasomatism; U-Pb geochronology of zircons in cratonic mantle xenoliths from Montana and Tanzania. *Proceedings of the VIIth International Kimberlite Conference*, vol 2, 728-735.

Sato, K., Katsura, T & Ito, E. (1997). Phase relations of natural phlogopite with and without enstatite up to 8 GPa: implications for mantle metasomatism. *Earth and Planetary Sciences* **146**, 511-526.

Scambos, T.A. & Farmer, G.L. (1988). Multiple source components for alkalic igneous rocks in the Wyoming Province: isotopic and trace element evidence from central Montana. *EOS Transactions of the American Geophysical Union* **69**, 1510.

Schneider, M.E. & Eggler, D.H. (1986). Fluids in equilibrium with peridotite minerals: implications for mantle metasomatism. *Geochimica et Cosmochimica Acta* **50**, 711-724.

Smith, D. & Riter, J.C.A. (1997). Genesis and evolution of low-Al orthopyroxene in spinel peridotite xenoliths, Grand Canyon field, Arizona, USA. *Contributions to Mineralogy and Petrology* **127**, 391-404.

Sun, S.-S. & McDonough, W.F. (1989). Chemical and isotopic systematics of oceanic basalts: implications for mantle composition and processes. In: Saunders, A.D. & Norry, M.J. (eds*) Magmatism in the Ocean Basins. Geological Society of London, Special Publication* **42**, 313-345.

Sweatman, T.R. & Long, J.V.P. (1969). Quantitative electron microanalysis of rock-forming minerals. *Journal of Petrology* **10**, 332-379.

Takahashi, E., Shimazaki, Y., Tsuzaki, Y. & Yoshida, H. (1993). Melting study of peridotite KLB-1 to 6.5 GPa, and the origin of basaltic magmas. *Philosophical Transactions of the Royal Society of London* **342**, 105-120.

Tatsumi, Y., Hamilton, D.H. & Nesbitt, R.W. (1986). Chemical characteristics of fluid phase released from a subducted lithosphere and origin of arc magmas: Evidence from high-pressure experiments and natural rocks. *Journal of Volcanology and Geothermal Research* **29**, 293-309.

Thirlwall, M.F. (1991). Long term reproducibility of multicollector Sr and Nd isotope ratio analysis. *Chemical Geology (Isotope Geoscience)* **94**, 85-104.

Ulmer, P. (1989). The dependence of the Fe^{2+}-Mg cation-partitioning between olivine and basaltic liquid on pressure, temperature and composition. *Contributions to Mineralogy and Petrology* **101**, 261-273.

Walter, M. J. (1998). Melting of garnet peridotite and the origin of komatiite and depleted lithosphere. *Journal of Petrology* **39**, 29-60.

Wiechert, U., Ionov, D.A. & Wedepohl, K.H. (1997). Spinel peridotite xenoliths from the Atsagin-Dush volcano, Dariganga lava plateau, Mongolia: a record of partial melting and cryptic metasomatism in the upper mantle. *Contributions to Mineralogy and Petrology* **126**, 345-364.

Wilshire, H.G. and Shervais, J.W. (1975). Al-augite and Cr-diopside ultramafic xenoliths in basaltic rocks from western United States. *Physics and Chemistry of the Earth* **9,** 257-272.

Witt-Eickschen, G. & Kramm , U. (1997). Mantle upwelling and metasomatism beneath Central Europe: geochemical and isotopic constraints from mantle xenoliths from the Rhön (Germany). *Journal of Petrology* **38**, 479-49.

Wooden, J.L. & Mueller, P.A. (1988). Pb, Sr, and Nd isotopic compositions of a suite of Late Archean igneous rocks, eastern Beartooth Mountains: implications for crust-mantle evolution. *Earth and Planetary Science Letters* **87**, 59-72.

You, C.-F., Castillo, P.R., Gieskes, J.M., Chan, L.H. & Spivack, A.J. (1996). Trace element behavior in hydrothermal experiments: Implications for fluid processes at shallow depths in subduction zones. *Earth and Planetary Science Letters* **140**, 41-52.

Figure captions

Fig. 1. Location map of the Bearpaw Mountains and other parts of the Montana high-K igneous province. Modified from Hearn (1989a).

Fig. 2. Photomicrographs of ultramafic xenoliths from the Bearpaw Mountains: (a) LSC 263, a porphyroclastic spinel peridotite tectonite, showing details of jagged "holly-leaf" Cr-spinels in a matrix of olivine and orthopyroxene, PPL, Field of view = 2mm; (b) WC 171, a porphyroclastic harzburgite, showing prominent white orthopyroxene porphyroclast in a matrix of neoblastic olivine (altered to serpentine), PPL, Field of view = 6mm; (c) LSC 197, a foliated mica websterite, showing tabular mica and elongate orthopyroxene crystals, PPL, Field of view = 6mm; (d) LSC 197, a foliated mica websterite, showing details of mica and orthopyroxene crystals, PPL, Field of view = 2mm; (e) LSC 188, a foliated mica websterite, showing parallel alignment of mica crystals in a matrix of clinopyroxene, PPL, Field of view = 2mm; (f) WC232, a cumulate mica dunite, consisting of olivine crystals (somewhat serpentinised) and anhedral interstitial phlogopite, PPL, Field of view = 6mm; (g) LSC 240, a cumulate mica lherzolite, showing olivine crystals poikilitically enclosed by phlogopite, PPL, Field of view = 2mm; (h) LSC 201, a cumulate mica wehrlite, showing clinopyroxene and olivine crystals poikilitically enclosed by phlogopite, PPL, Field of view = 2mm; (i) LSC 220, a cumulate mica wehrlite, showing clinopyroxene and olivine enclosed by phlogopite, PPL, Field of view = 2mm; (j) LSC 199, a cumulate mica clinopyroxenite, showing

clinopyroxene and plates of poikilitic phlogopite, with interstitial phlogopite, PPL, Field of view = 2mm.

Fig. 3. Fo content of olivine vs. NiO content of ultramafic xenoliths of the Bearpaw Mountains. Data from Table 2. Field of non-cratonic mantle olivines from McDonough & Rudnick (1998). Field of olivine in cratonic mantle spinel peridotites from Bernstein et al (1998) and Lee and Rudnick (1999). Field of olivines in host minettes from Macdonald *et al*. (1992).

Fig. 4. (a) 100Cr/(Cr+Al) vs. 100Mg/(Mg+Fe^{2+}) variations in spinels from ultramafic xenoliths of the Bearpaw Mountains. (b) 100Cr/(Cr+Al) in spinels plotted against Fo content of olivines. Data from Tables 2 and 3. Field of mantle peridotites from McDonough & Rudnick (1998). Field of spinels and olivines in cratonic mantle spinel peridotites from Bernstein et al (1998) and Lee and Rudnick (1999).

Fig. 5. Compositions of orthopyroxenes (a) and clinopyroxenes (b) in Bearpaw ultramafic xenoliths. Composition of clinopyroxene phenocrysts in host minettes from Macdonald *et al*. (1992). Fields of pyroxenes in mantle peridotites from McDonough & Rudnick (1998). Field of pyroxenes in cratonic mantle spinel peridotites from Bernstein et al (1998) and Lee and Rudnick (1999). Data from Tables 4 and 5.

Fig. 6. Comparison of the compositions of phlogopites in Bearpaw ultramafic xenoliths with the composition of phenocrysts in host minettes (Macdonald *et al*., 1992). Field of phlogopite in mantle peridotites from McDonough & Rudnick (1998). Symbols as for Figure 5. Data from Table 6.

Fig. 7. Selected major element oxides vs MgO for Bearpaw ultramafic xenoliths (data from Tables 8-10). Field of off-craton spinel peridotites from Downes (2001). Field of cratonic mantle spinel peridotites from Lee and Rudnick (1999). Note logarithmic scale for K_2O abundances.

Fig. 8. Selected trace elements vs MgO for Bearpaw ultramafic xenoliths (data from Tables 8-10). Field for spinel peridotites from Downes (2001). Note logarithmic scale for Rb abundances.

Fig. 9. Chondrite-normalised whole-rock REE patterns for Bearpaw ultramafic xenoliths: (a) tectonite peridotites; (b) cumulate peridotites and pyroxenites; (c) other rock-types. Normalising factors from Nakamura (1974). Data from Table 11.

Fig. 10. Mantle-normalised trace element abundances for whole rock Bearpaw ultramafic xenoliths. Normalising values for primitive mantle from Sun & McDonough (1989). (a) tectonite peridotites; (b) cumulate peridotites and pyroxenites (thick solid line = composition of Bearpaw mountains minette (Macdonald *et al*., 1992); (c) tectonite harzburgites with white orthopyroxene, and foliated mica websterites. Data analysed by solution ICP-MS (Table 11), except for Zr in websterites (XRF Zr value from Table 10 substituted).

Fig. 11. Chondrite-normalised REE patterns from Bearpaw ultramafic xenoliths: (a) clinopyroxenes from tectonite peridotites (LA-ICP-MS data from Table 12); (b) cumulate xenoliths (LA-ICP-MS data from Table 12); (c) calculated melts in equilibrium with clinopyroxenes from cumulate xenoliths LSC 237 and LSC 201, compared with whole-rock analysis of Bearpaw mountains minette (Macdonald *et al*., 1992). Normalising factors from Nakamura (1974).

Fig. 12. Mantle-normalised trace element abundances for clinopyroxenes from Bearpaw ultramafic xenoliths (LA-ICP-MS data). Normalising values for primitive mantle from Sun & McDonough (1989). (a) tectonite peridotites; (b) cumulate xenoliths.

Fig. 13. Mantle-normalised trace element abundances for clinopyroxenes (LA-ICP-MS data – Table 12) compared with whole-rock compositions (solution ICP-MS data – Table 11, except for Zr in websterite LSC 188 (XRF Zr value from Table 10 substituted).

Fig. 14. Sr-Nd isotope diagram for ultramafic xenoliths from the Bearpaw Mountains (data from Table 12), compared with spinel peridotite xenoliths from non-cratonic lithospheric mantle of western Europe (Downes, 2001) and local lithospheric mantle xenoliths from Eagle Buttes and Highwood Mountains (Carlson & Irving, 1994) and Missouri Breaks kimberlites (Carlson *et al*., 1999). Field of host minettes from Macdonald *et al*., 1992).

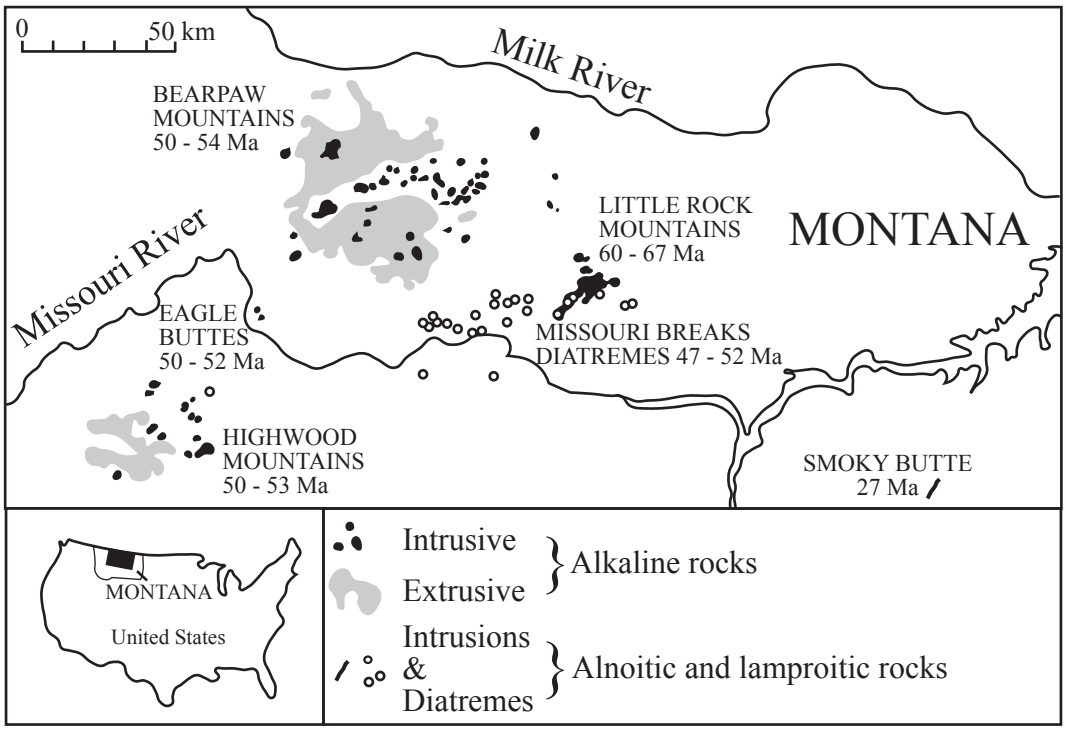
0
50 km
Milk River
BEARPAW
MOUNTAINS
50 - 54 Ma
LITTLE ROCK
MOUNTAINS
60 - 67 Ma
MONTANA
Missouri River
EAGLE
BUTTES
50 - 52 Ma
MISSOURI BREAKS
DIATREMES 47 - 52 Ma
HIGHWOOD
MOUNTAINS
50 - 53 Ma
SMOKY BUTTE
27 Ma
MONTANA
United States
Intrusive
Extrusive
Alkaline rocks
Intrusions
&
Diatremes
Alnoitic and lamproitic rocks

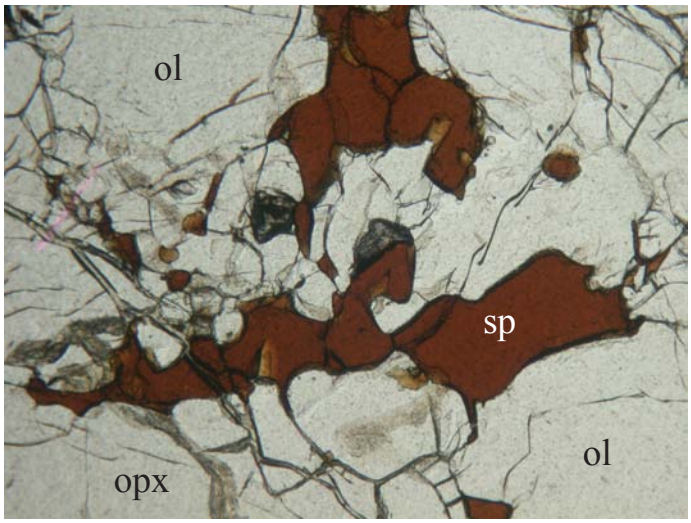

(a)

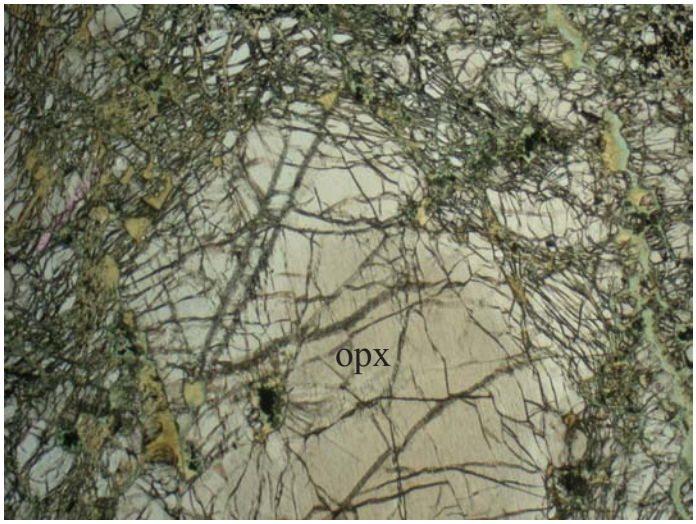

(b)

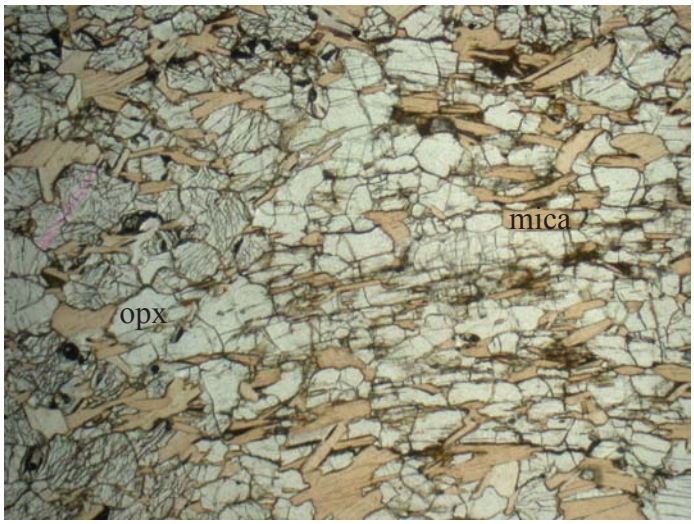

(c)

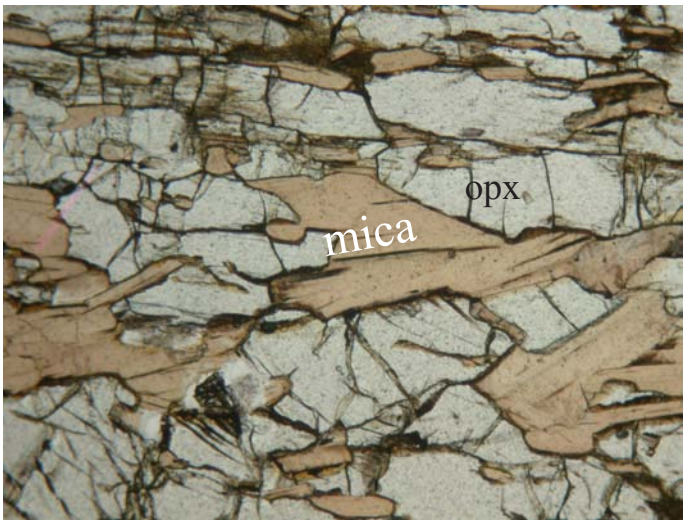

(d)

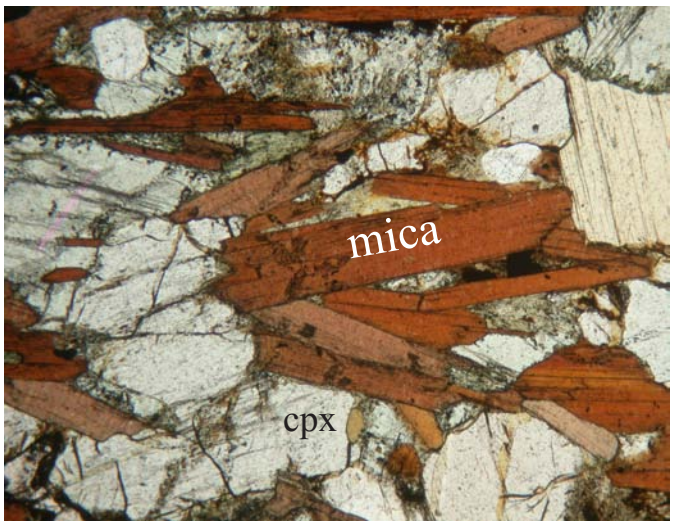

(e)

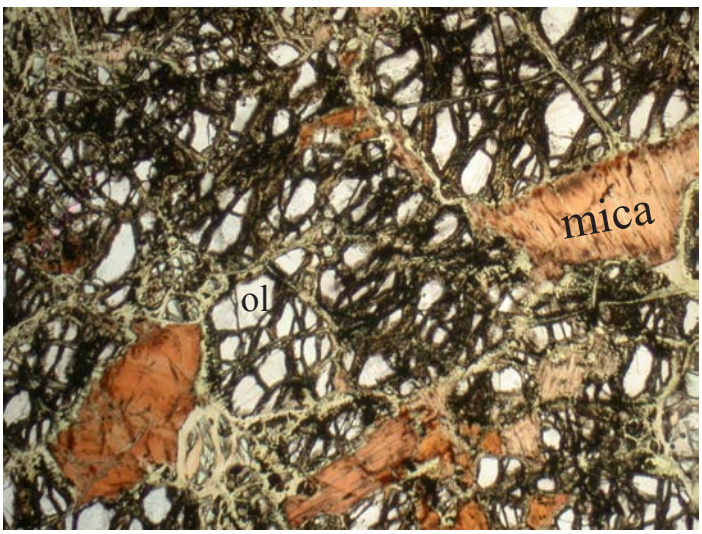

(f)

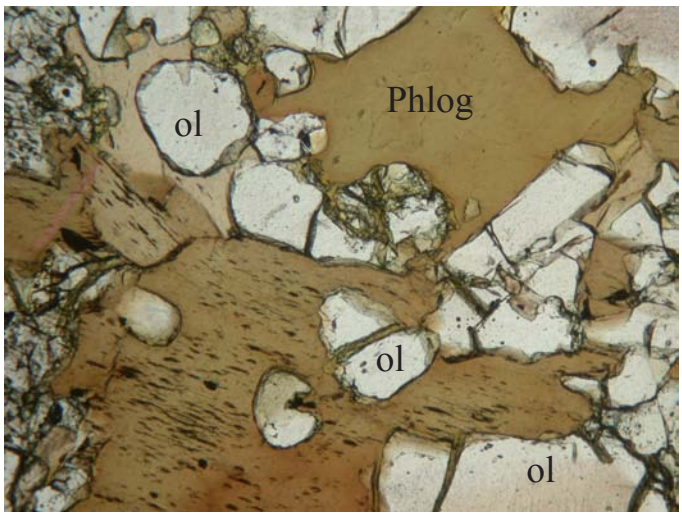

(g)

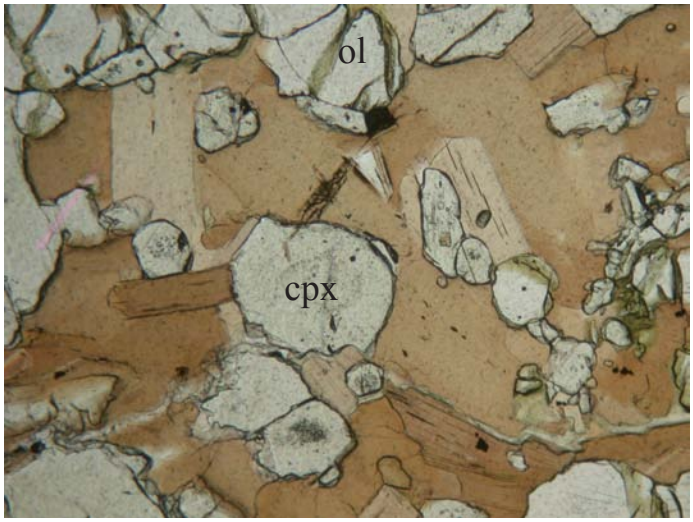

(h)

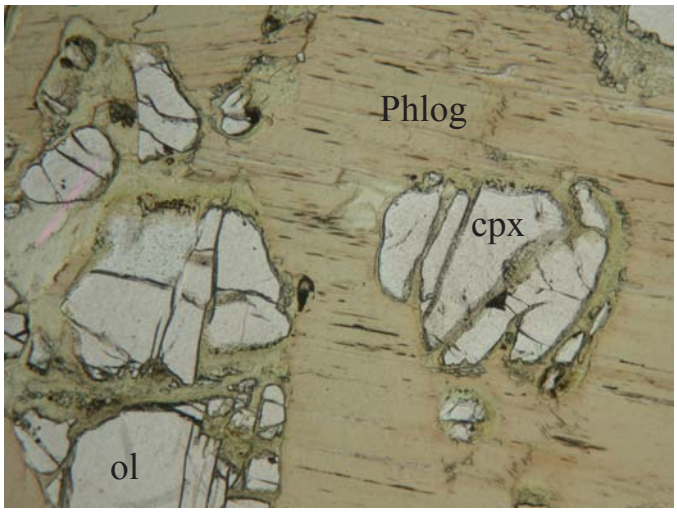

(i)

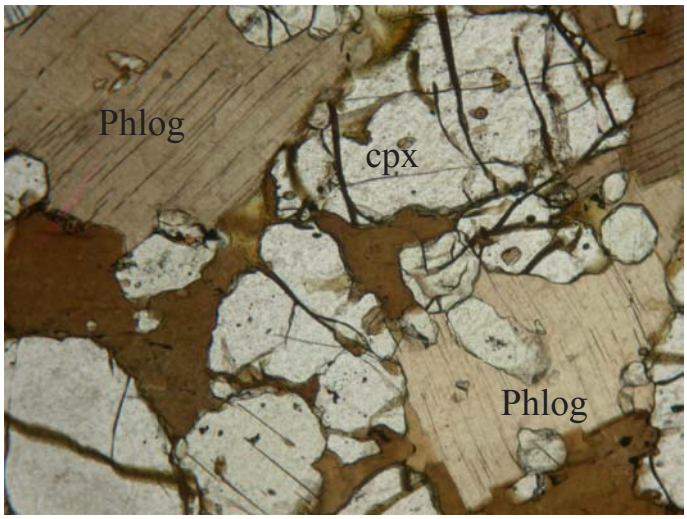

(j)

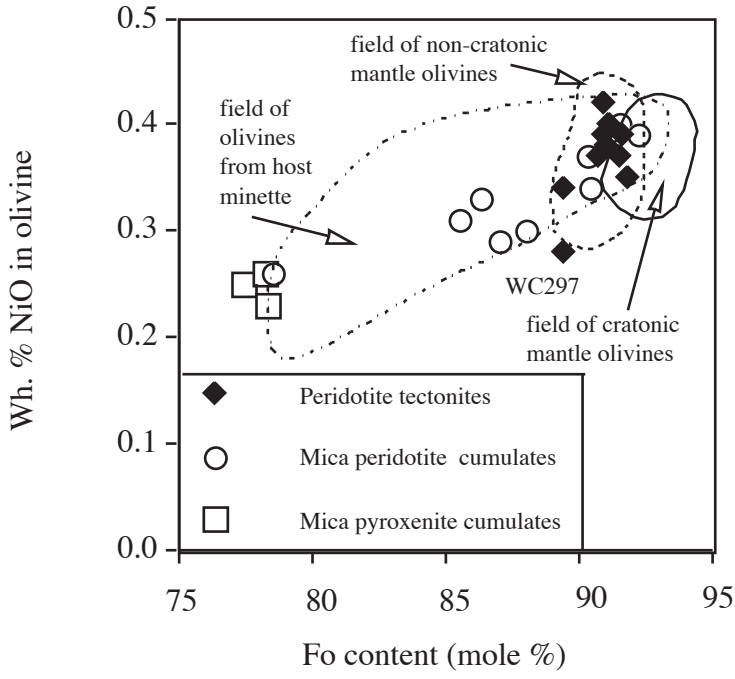
0.5
0.4
0.3
0.2
0.1
0.0
Wh. % NiO in olivine
field of non-cratonic
mantle olivines
field of
olivines
from host
minette
WC297
field of cratonic
mantle olivines
Peridotite tectonites
Mica peridotite cumulates
Mica pyroxenite cumulates
75
80
85
90
95
Fo content (mole %)

Figure 3

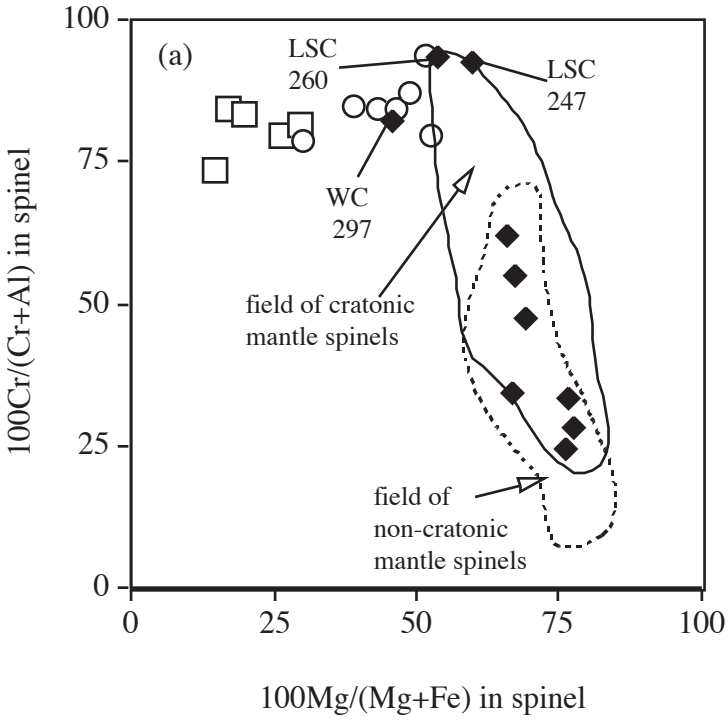
(a)
LSC
260
LSC
247
WC
297
field of cratonic
mantle spinels
field of
non-cratonic
mantle spinels
100Cr/(Cr+Al) in spinel
100Mg/(Mg+Fe) in spinel
0
25
50
75
100

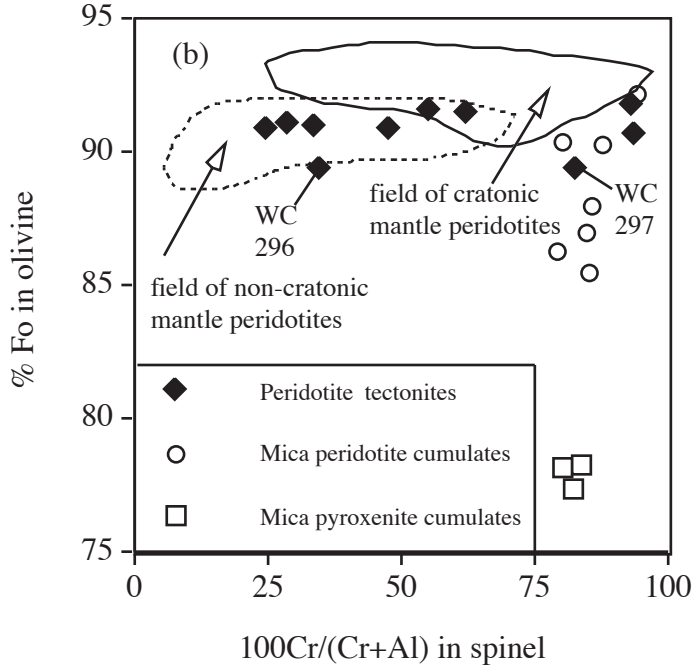
(b)
WC
296
field of cratonic
mantle peridotites
WC
297
field of non-cratonic
mantle peridotites
Peridotite tectonites
Mica peridotite cumulates
Mica pyroxenite cumulates
% Fo in olivine
100Cr/(Cr+Al) in spinel
75
80
85
90
95
0
25
50
75
100

Figure 4

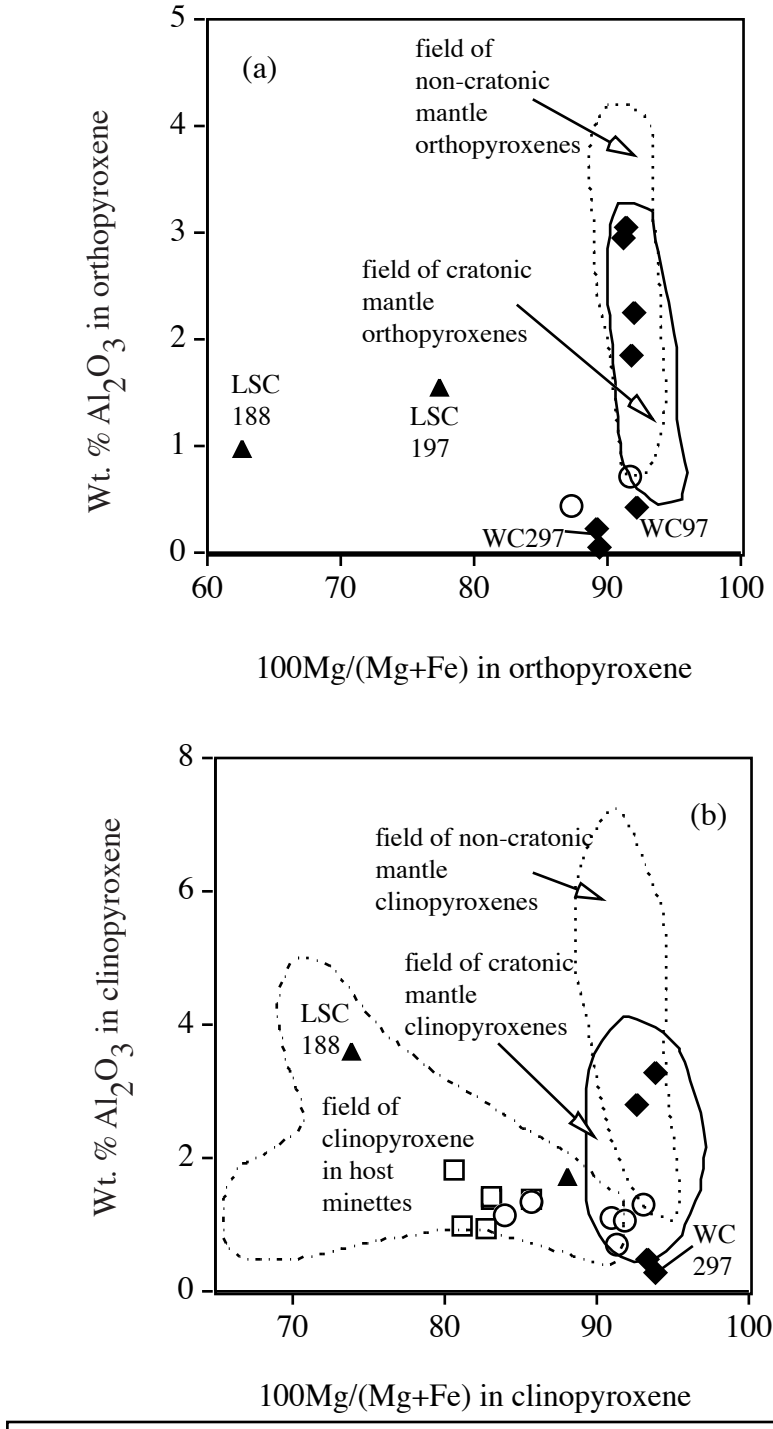
(a)
field of non-cratonic mantle orthopyroxenes
field of cratonic mantle orthopyroxenes
LSC 188
LSC 197
WC297
WC97
Wt. % Al_2O_3 in orthopyroxene
100Mg/(Mg+Fe) in orthopyroxene
(b)
field of non-cratonic mantle clinopyroxenes
field of cratonic mantle clinopyroxenes
LSC 188
field of clinopyroxene in host minettes
WC 297
Wt. % Al_2O_3 in clinopyroxene
100Mg/(Mg+Fe) in clinopyroxene
Peridotite tectonites
Mica peridotite cumulates
Mica pyroxenite cumulates
Mica websterites

Figure 5

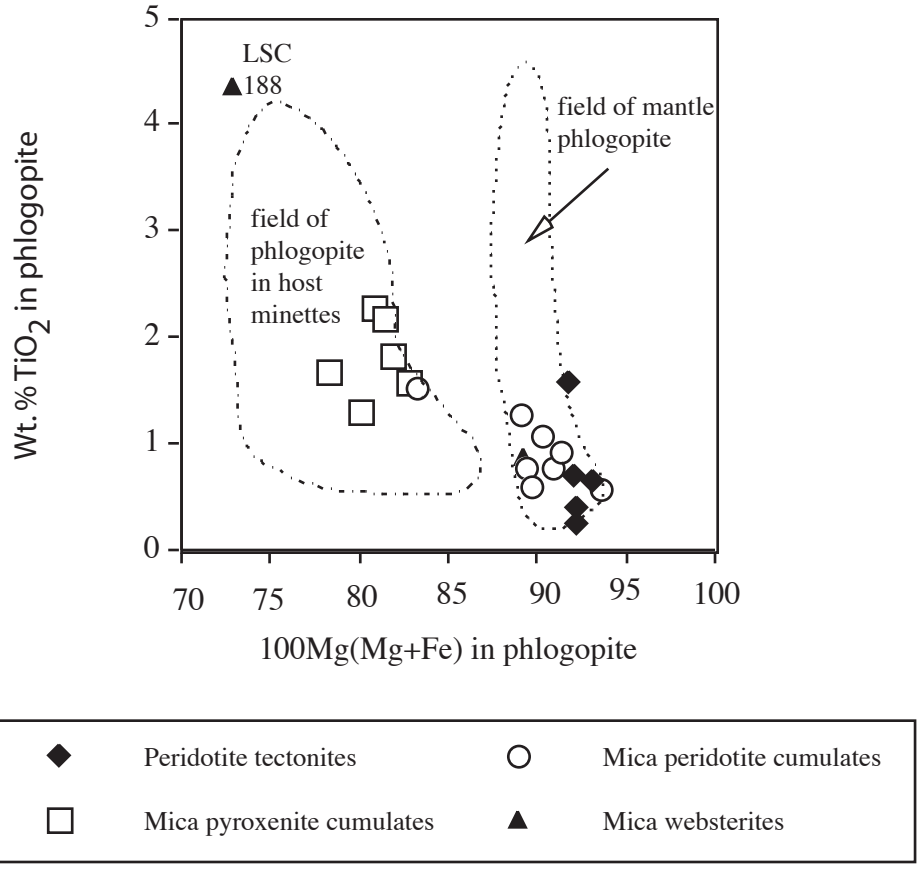
5
4
3
2
1
0
LSC
188
field of mantle
phlogopite
field of
phlogopite
in host
minettes
Wt. % TiO2 in phlogopite
70
75
80
85
90
95
100
100Mg(Mg+Fe) in phlogopite
Peridotite tectonites
Mica peridotite cumulates
Mica pyroxenite cumulates
Mica websterites

Figure 6

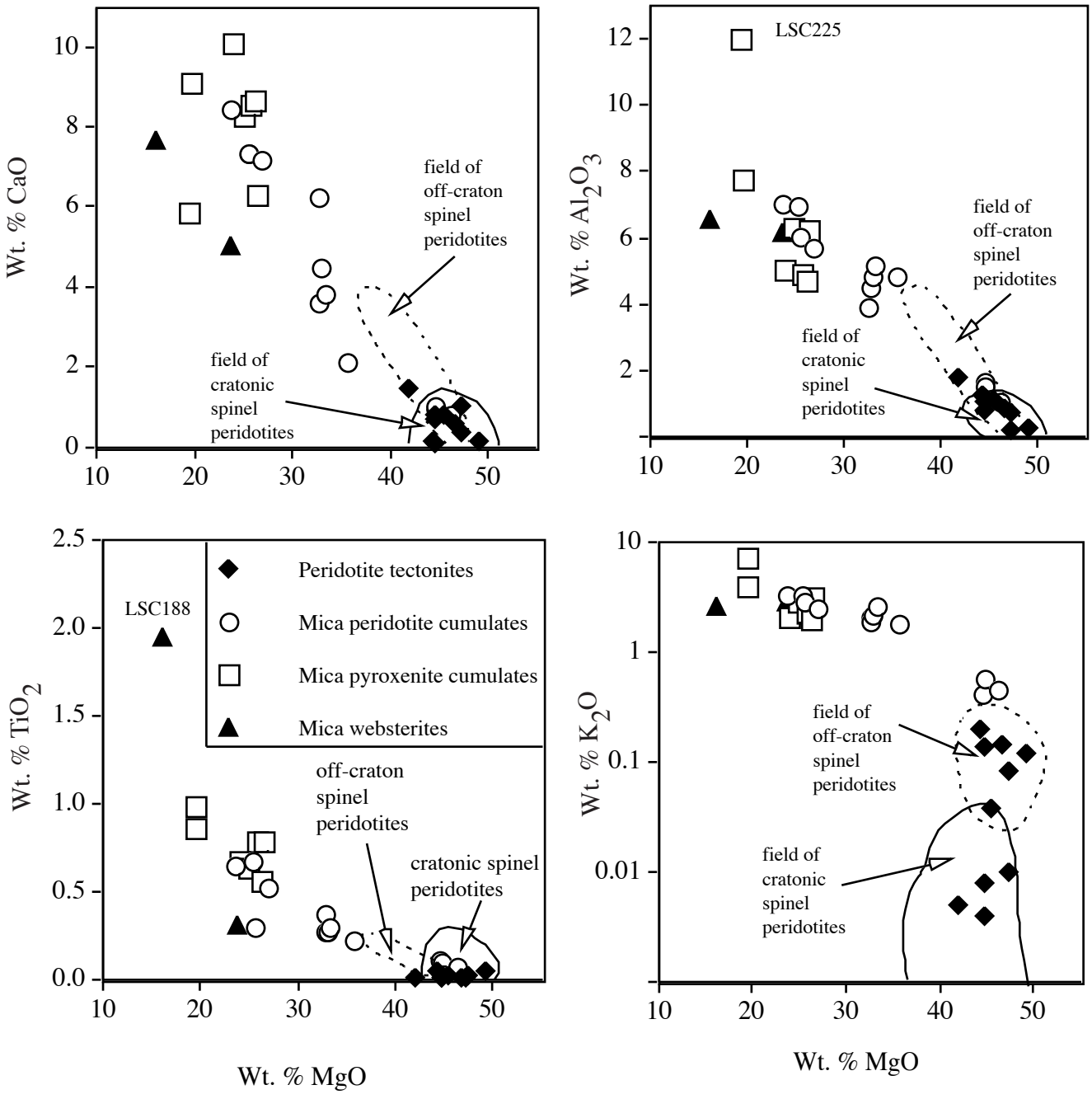
Wt. % CaO
field of off-craton spinel peridotites
field of cratonic spinel peridotites
LSC225
Wt. % Al_2O_3
field of off-craton spinel peridotites
field of cratonic spinel peridotites
LSC188
Peridotite tectonites
Mica peridotite cumulates
Mica pyroxenite cumulates
Mica websterites
Wt. % TiO_2
off-craton spinel peridotites
cratonic spinel peridotites
Wt. % MgO
Wt. % K_2O
field of off-craton spinel peridotites
field of cratonic spinel peridotites
Wt. % MgO

Figure 7

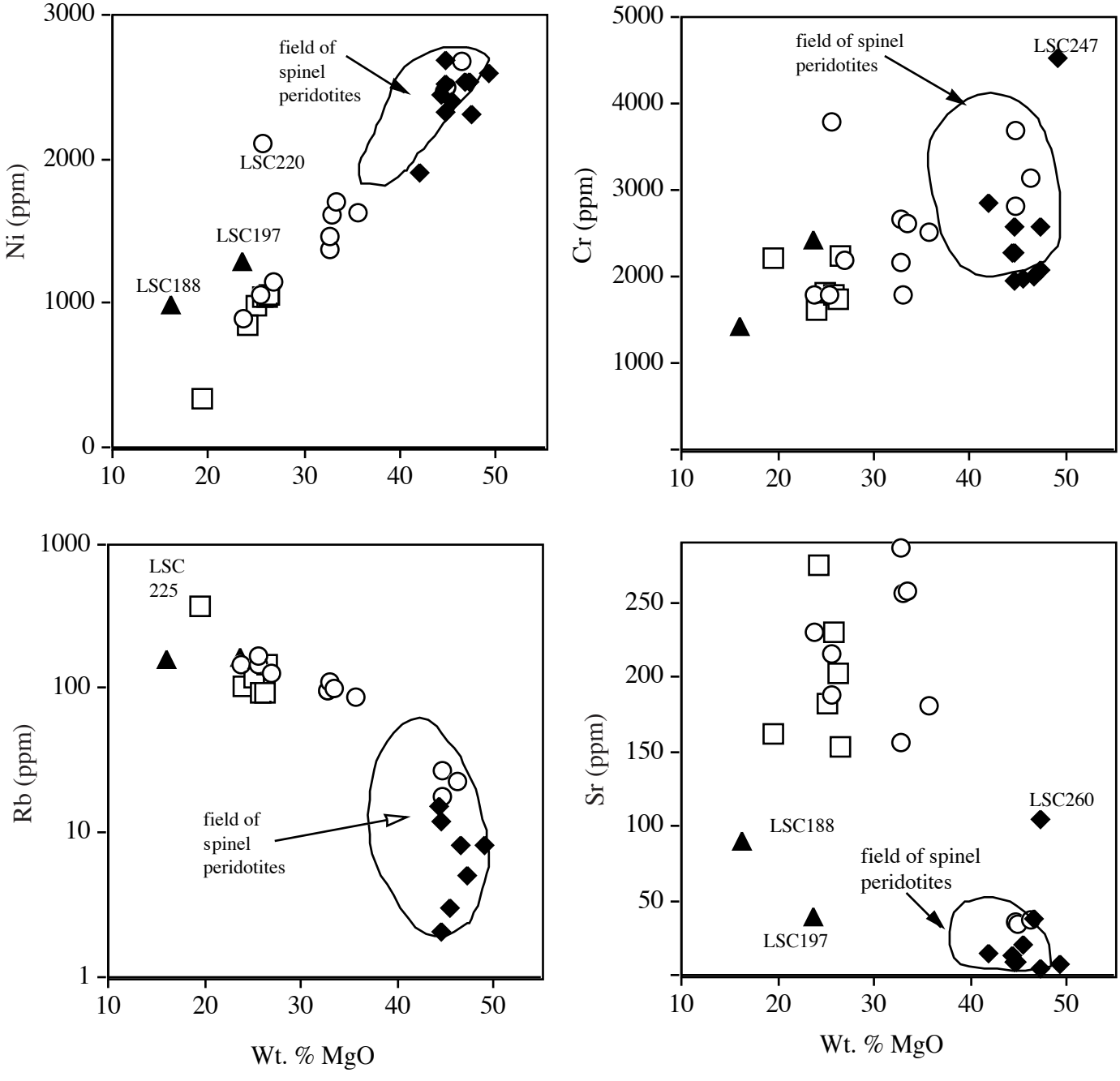
Ni (ppm)
3000
2000
1000
0
10
20
30
40
50
field of spinel peridotites
LSC220
LSC197
LSC188
Cr (ppm)
5000
4000
3000
2000
1000
field of spinel peridotites
LSC247
Rb (ppm)
1000
100
10
1
LSC 225
field of spinel peridotites
Wt. % MgO
Sr (ppm)
250
200
150
100
50
LSC260
LSC188
field of spinel peridotites
LSC197
Wt. % MgO

Figure 8

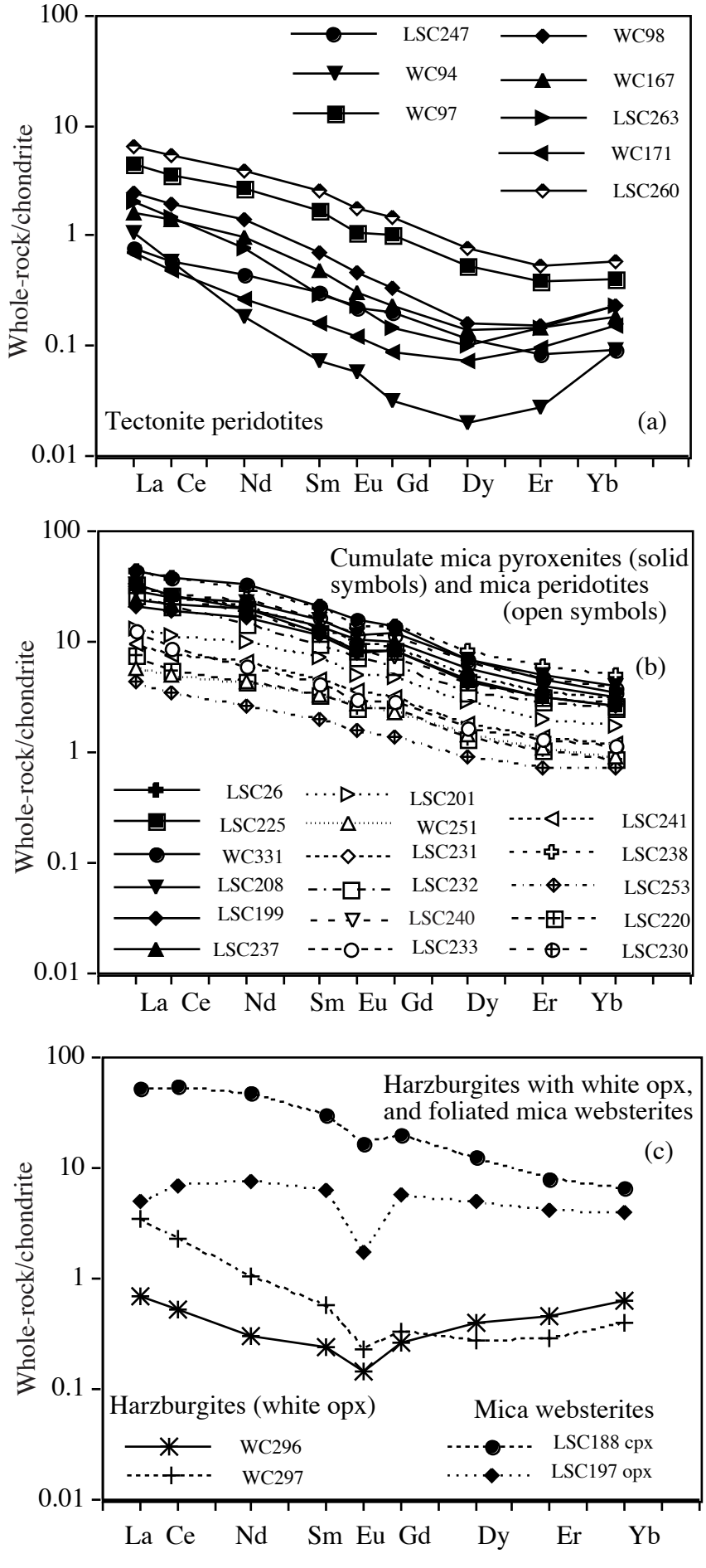
100
10
1
0.1
0.01
Whole-rock/chondrite
LSC247
WC98
WC94
WC167
WC97
LSC263
WC171
LSC260
Tectonite peridotites
(a)
La Ce Nd Sm Eu Gd Dy Er Yb
Cumulate mica pyroxenites (solid symbols) and mica peridotites (open symbols)
(b)
LSC26
LSC201
LSC225
WC251
LSC241
WC331
LSC231
LSC238
LSC208
LSC232
LSC253
LSC199
LSC240
LSC220
LSC237
LSC233
LSC230
Harzburgites with white opx, and foliated mica websterites
(c)
Harzburgites (white opx)
WC296
WC297
Mica websterites
LSC188 cpx
LSC197 opx

Figure 9

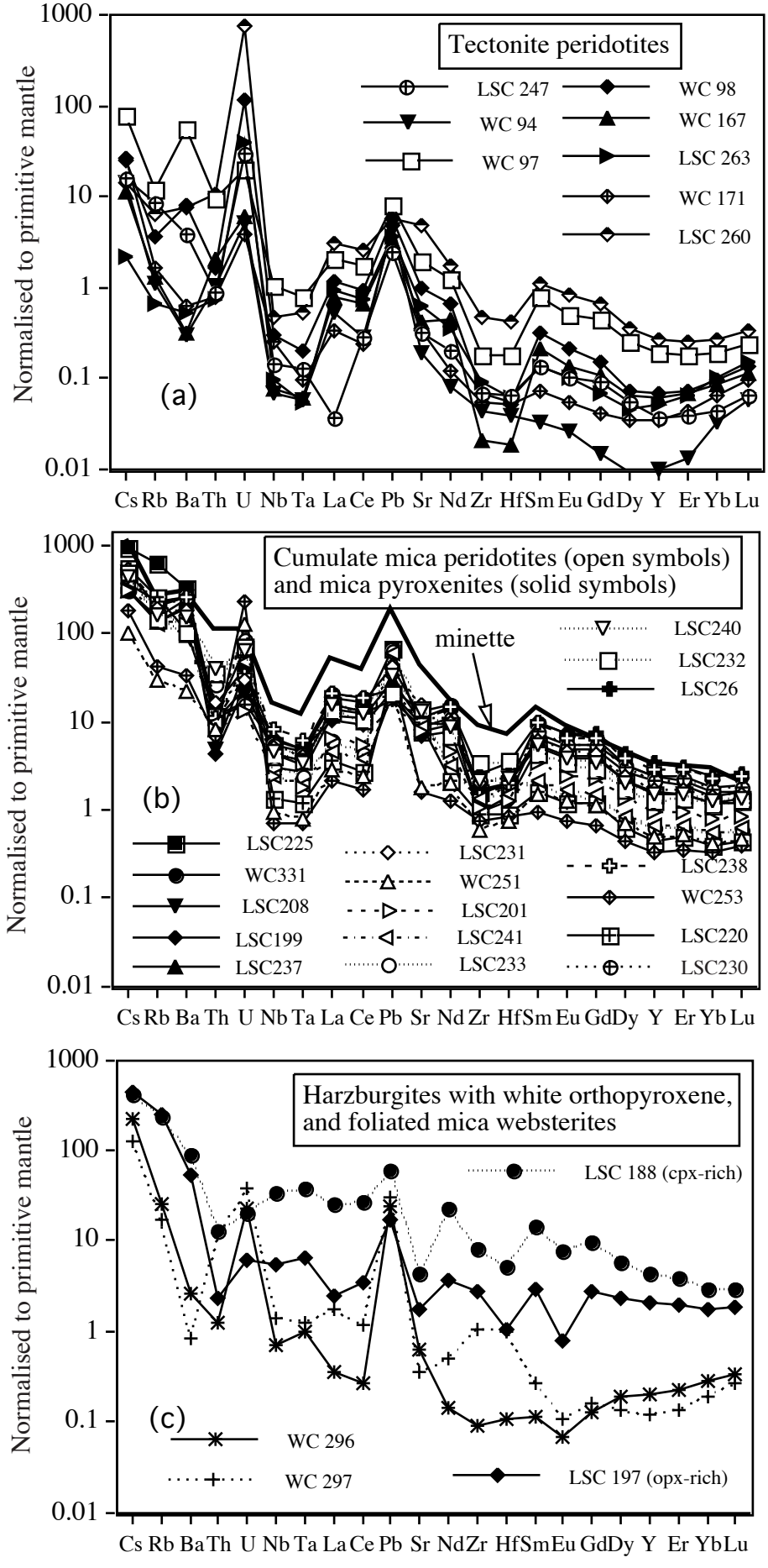
Tectonite peridotites
LSC 247
WC 98
WC 94
WC 167
WC 97
LSC 263
WC 171
LSC 260
(a)
Normalised to primitive mantle
1000
100
10
1
0.1
0.01
Cs Rb Ba Th U Nb Ta La Ce Pb Sr Nd Zr Hf Sm Eu Gd Dy Y Er Yb Lu
Cumulate mica peridotites (open symbols)
and mica pyroxenites (solid symbols)
minette
LSC240
LSC232
LSC26
(b)
LSC225
LSC231
LSC238
WC331
WC251
WC253
LSC208
LSC201
LSC199
LSC241
LSC220
LSC237
LSC233
LSC230
Harzburgites with white orthopyroxene,
and foliated mica websterites
LSC 188 (cpx-rich)
(c)
WC 296
WC 297
LSC 197 (opx-rich)

Figure 10

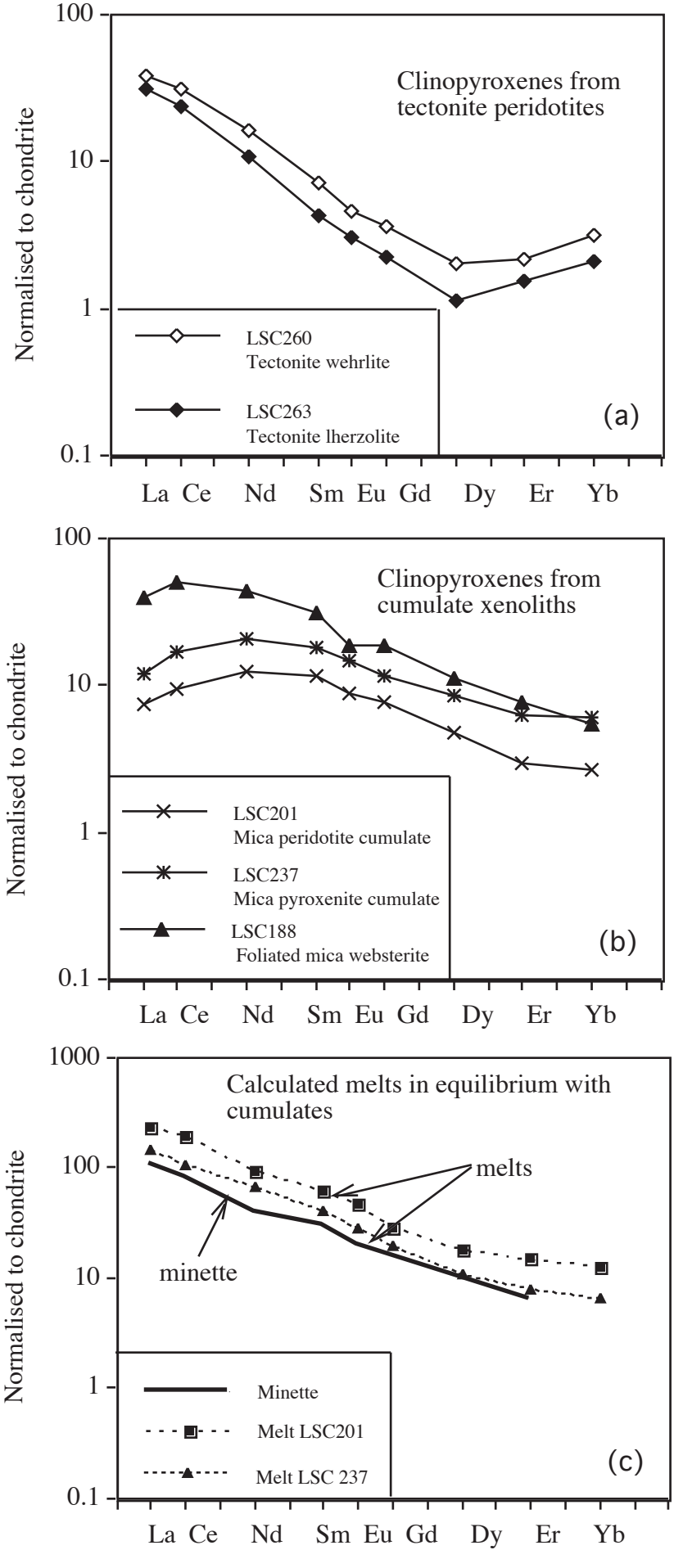
100
10
1
0.1
Normalised to chondrite
Clinopyroxenes from
tectonite peridotites
LSC260
Tectonite wehrlite
LSC263
Tectonite lherzolite
(a)
La Ce Nd Sm Eu Gd Dy Er Yb
100
10
1
0.1
Normalised to chondrite
Clinopyroxenes from
cumulate xenoliths
LSC201
Mica peridotite cumulate
LSC237
Mica pyroxenite cumulate
LSC188
Foliated mica websterite
(b)
La Ce Nd Sm Eu Gd Dy Er Yb
1000
100
10
1
0.1
Normalised to chondrite
Calculated melts in equilibrium with
cumulates
melts
minette
Minette
Melt LSC201
Melt LSC 237
(c)
La Ce Nd Sm Eu Gd Dy Er Yb

Figure 11

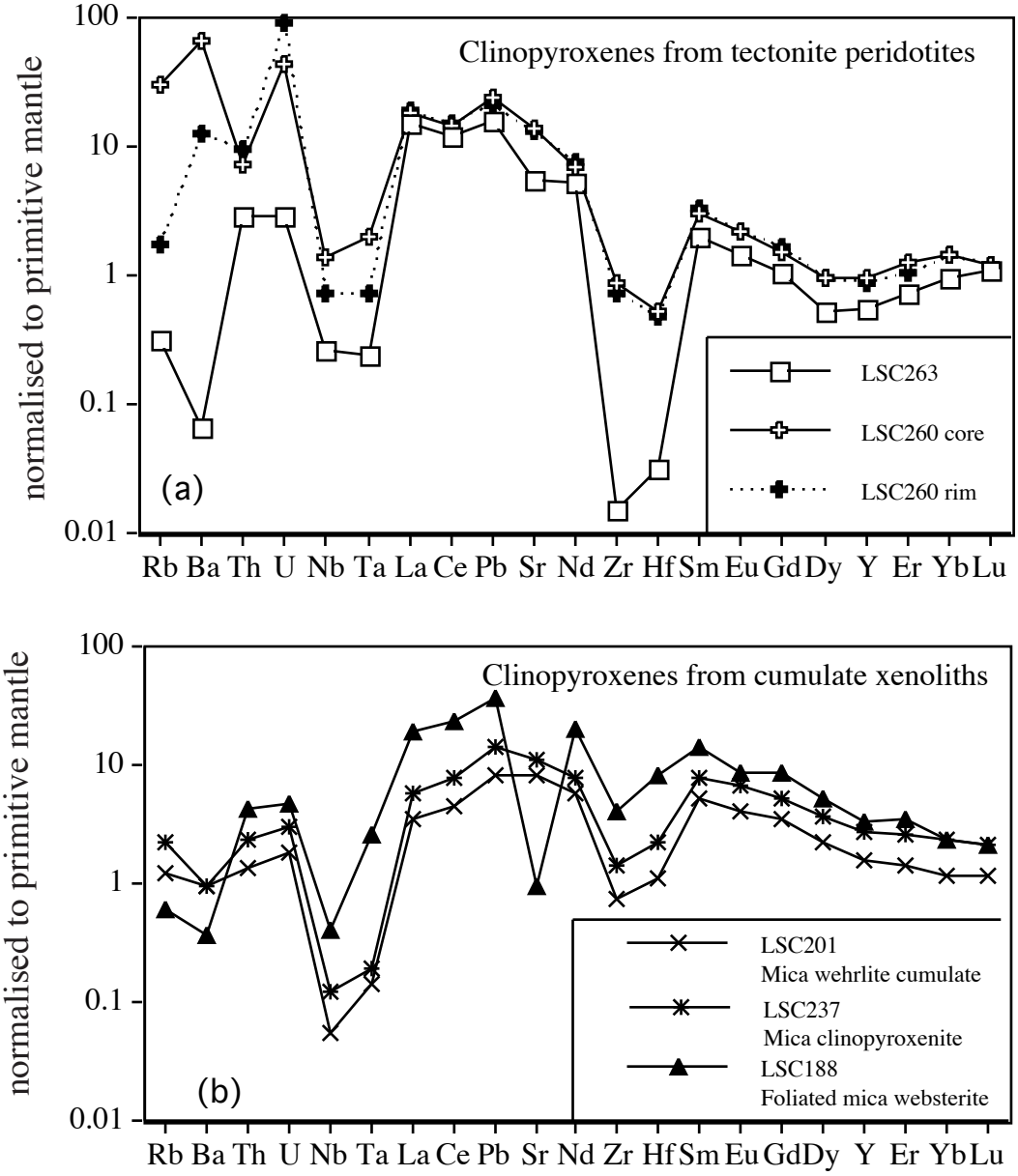
Clinopyroxenes from tectonite peridotites
normalised to primitive mantle
100
10
1
0.1
0.01
(a)
LSC263
LSC260 core
LSC260 rim
Rb Ba Th U Nb Ta La Ce Pb Sr Nd Zr Hf Sm Eu Gd Dy Y Er Yb Lu
Clinopyroxenes from cumulate xenoliths
normalised to primitive mantle
100
10
1
0.1
0.01
(b)
LSC201
Mica wehrlite cumulate
LSC237
Mica clinopyroxenite
LSC188
Foliated mica websterite
Rb Ba Th U Nb Ta La Ce Pb Sr Nd Zr Hf Sm Eu Gd Dy Y Er Yb Lu

Figure 12

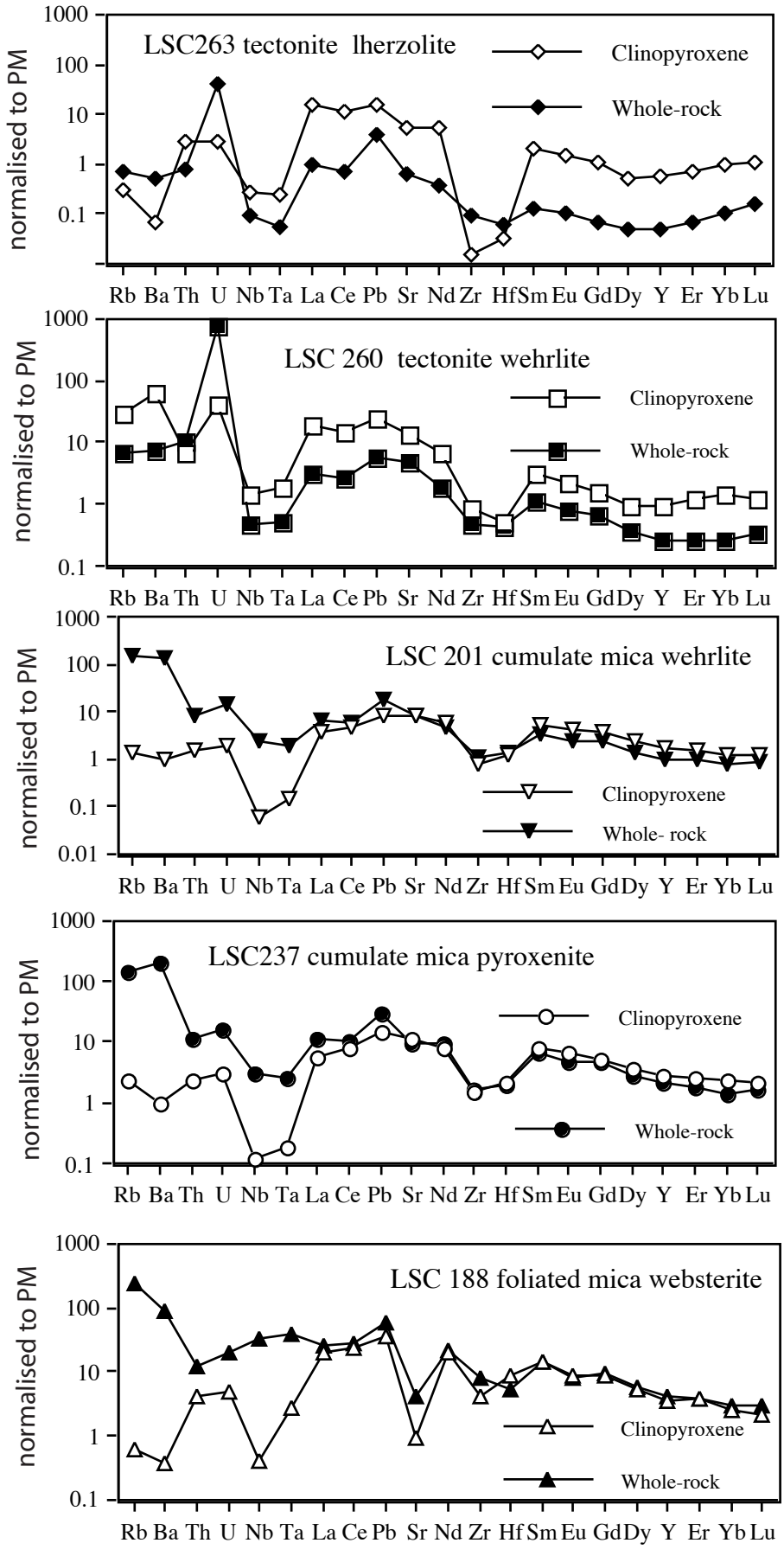
LSC263 tectonite lherzolite
Clinopyroxene
Whole-rock
LSC 260 tectonite wehrlite
Clinopyroxene
Whole-rock
LSC 201 cumulate mica wehrlite
Clinopyroxene
Whole- rock
LSC237 cumulate mica pyroxenite
Clinopyroxene
Whole-rock
LSC 188 foliated mica websterite
Clinopyroxene
Whole-rock
normalised to PM
1000
100
10
1
0.1
0.01
Rb Ba Th U Nb Ta La Ce Pb Sr Nd Zr Hf Sm Eu Gd Dy Y Er Yb Lu

Figure 13

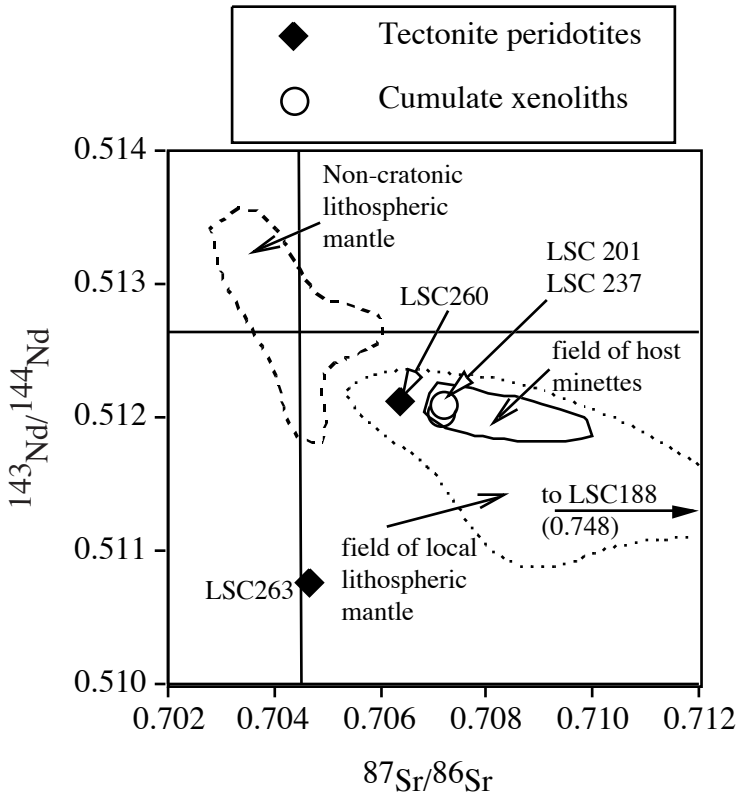
Tectonite peridotites
Cumulate xenoliths
0.514
0.513
0.512
0.511
0.510
0.702
0.704
0.706
0.708
0.710
0.712
$^{143}Nd/^{144}Nd$
$^{87}Sr/^{86}Sr$
Non-cratonic lithospheric mantle
LSC 201
LSC 237
LSC260
field of host minettes
to LSC188
(0.748)
field of local lithospheric mantle
LSC263

Figure 14

Table 1. Modal analyses of ultramafic xenoliths from the Bearpaw Mountains.

Sample no.	Lithology	Ol	Sp	Opx	Cpx	Phlog
Spinel peridotite tectonites						
LSC 247	Dunite	96.8	3.2	-	-	tr
WC 94	Harzburgite	93.5	1.5	4.4	-	0.6
WC97	Harzburgite	90.1	1.5	8.5	tr	tr
WC98	Harzburgite	80.7	0.8	18.4	tr	tr
WC 167	Harzburgite	89.6	1.4	6.5	2.6	-
LSC 263	Lherzolite	59.5	1.3	31.1	7.9	-
WC 171	Harzburgite	64.1	tr	31.1	4.8	-
LSC 260	Wehrlite	81.1	1.2	-	16.8	0.8
Spinel peridotite tectonites with white orthopyroxene						
WC 296	Harzburgite	74.1	1.2	24.7	-	tr
WC 297	Harzburgite	82.3	2.5	12.4	-	2.8
Mica websterites (foliated)*						
LSC 197	Opx-rich	-	-	51.0	20.4	28.7
LSC 188†	Cpx rich	-	-	6.0	54.4	36.0
Mica peridotite cumulates‡						
WC 253	Mica wehrlite	75.5	0.8	tr	7.0	16.7
WC 232	Mica dunite	88.0	0.5	-	-	11.5
WC251	Mica wehrlite	78.7	0.3	0.7	4.6	15.7
LSC 241	Mica wehrlite	36.0	tr	-	15.4	48.5
LSC 240	Mica lherzolite	32.2	tr	10.1	18.7	39.0
LSC 201	Mica wehrlite	39.4	tr	-	34.5	26.1
LSC 233	Mica dunite	34.8	0.5	1.0	2.0	41.7
LSC 232	Mica lherzolite	32.1	0.3	7.7	17.9	42.0
LSC 231	Mica lherzolite	30.5	tr	7.6	24.5	37.4
LSC 238	Mica wehrlite	35.4	0.1	-	15.9	48.6
LSC 220	Mica wehrlite	31.0	tr	2.8	27.0	39.2
LSC 230	Mica wehrlite	20.3	tr	3.6	35.9	40.3
Mica clinopyroxenite cumulates‡						
LSC 237	Mica clinopyroxenite	14.1	0.9	-	54.7	30.3
LSC 199	Mica clinopyroxenite	18.9	0.7	-	36.8	43.6
LSC 26	Mica clinopyroxenite	29.7	0.4	-	39.6	30.3
LSC 208	Mica clinopyroxenite	18.3	1.3	-	39.4	41.0
WC 331	Mica clinopyroxenite	10.6	tr	-	48.6	40.8
LSC 204	Mica clinopyroxenite	7.7	0.7	-	39.0	52.6
LSC 225	Glimmerite	-	-	-	19.2	80.8

Ol = olivine; Sp = spinel; Opx = orthopyroxene; Cpx = clinopyroxene; Phlog = phlogopite; tr = present in trace amounts (<0.1%); * websterites contain rare zircon; † LSC 188 contains very rare monazite; ‡ all cumulates contain apatite.

Table 2. Compositional data for olivines from ultramafic xenoliths from the Bearpaw Mountains.

Sample no:	LSC247	WC94	WC97	WC98	WC167	LSC263	WC171	LSC260	WC296	WC297
Lithology:	T D	T H	T H	T H	T H	T L	T H	T W	T H O	T H O
SiO_2	40.63	40.34	40.24	40.65	40.65	40.73	41.10	40.86	40.14	40.35
Al_2O_3	0.02	0.04	0.03	0.04	0.04	0.05	0.05	0.04	0.06	0.03
FeO	8.01	8.20	8.25	8.83	8.69	8.92	8.94	9.12	10.30	10.42
MnO	0.12	0.10	0.12	0.14	0.12	0.12	0.13	0.16	0.41	0.26
MgO	50.60	50.46	50.11	50.36	49.97	49.80	49.93	49.78	48.88	49.46
NiO	0.35	0.39	0.37	0.38	0.40	0.39	0.42	0.37	0.34	0.28
CaO	0.06	0.04	0.06	0.09	0.05	0.01	0.05	0.02	0.02	0.06
Total	99.79	99.56	99.18	100.47	99.91	100.02	100.62	100.34	100.13	100.85
% Forsterite	91.8	91.6	91.5	91.0	91.1	90.9	90.9	90.7	89.4	89.4

Sample no:	WC253	WC232	WC 251	LSC241	LSC 240	LSC 201	LSC 238	LSC 220	LSC 237	LSC 208	WC331
Lithology	C M W	C M D	C M W	C M W	C M W	C M W	C M W	C M W	C M W	C M P	C M P
SiO_2	40.31	40.71	40.40	40.10	39.89	39.86	38.76	40.58	38.82	38.40	38.63
Al_2O_3	0.06	0.04	0.04	0.04	0.04	0.07	0.05	0.06	0.12	0.06	0.05
FeO	9.53	7.74	9.38	11.62	13.16	13.92	19.97	8.31	20.22	20.81	20.33
MnO	0.14	0.14	0.14	0.17	0.21	0.25	0.43	0.11	0.38	0.41	0.40
MgO	49.59	51.20	49.45	47.81	46.67	46.12	40.89	50.06	40.70	40.00	41.27
NiO	0.37	0.39	0.34	0.30	0.33	0.31	0.26	0.40	0.26	0.25	0.23
CaO	0.06	0.05	0.03	0.06	0.04	0.07	0.07	0.06	0.10	0.09	0.12
Total	100.04	100.26	99.77	100.10	100.34	100.59	100.42	99.59	100.59	100.02	101.04
% Forsterite	90.3	92.2	90.4	88.0	86.3	85.5	78.5	91.5	78.2	77.4	78.3

Abbreviations: T = tectonite; C = cumulate; D = dunite; H = harzburgite; L = lherzolite; W = wehrlite;
O = contains white orthopyroxene; M = mica; P = pyroxenite

Table 3. Compositional data for spinels from ultramafic xenoliths from the Bearpaw Mountains.

Sample no:	LSC247	WC94	WC97	WC98	WC167	LSC263	LSC171	LSC260	WC296	WC297	WC235	WC232
Lithology:	T D	T H	T H	T H	T H	T L	T H	T W	T H O	T H O	C M W	C M D
SiO_2	0.13	0.12	0.15	0.15	0.09	0.06	0.16	0.13	0.16	0.13	0.18	0.17
TiO_2	0.84	0.01	0.07	0.04	<0.01	0.01	0.02	0.59	0.25	0.45	0.45	1.08
Al_2O_3	3.25	22.80	19.15	37.76	41.53	45.19	28.02	2.93	34.75	7.51	5.85	2.59
Cr_2O_3	61.95	41.22	46.65	28.30	24.47	21.77	37.52	60.37	27.05	51.98	59.37	58.57
V_2O_3	0.11	0.19	0.26	0.10	0.09	0.12	0.13	0.35	0.14	0.11	0.12	0.12
FeO	19.92	19.16	18.01	13.96	13.23	12.08	16.81	22.59	19.88	28.69	23.54	25.16
MnO	0.31	0.19	0.25	0.12	0.14	0.16	0.18	0.36	0.43	0.58	0.35	0.35
MgO	11.64	14.58	14.04	18.05	18.36	18.12	15.43	10.28	15.09	8.82	9.47	9.78
NiO	0.15	0.20	0.15	0.25	0.29	0.22	0.17	0.11	0.23	0.15	0.09	0.14
ZnO	0.10	0.08	0.10	0.09	0.09	0.31	0.07	0.11	0.14	0.34	0.17	0.15
Total	98.40	98.58	98.88	98.84	98.31	98.03	98.54	97.89	98.16	98.76	99.61	98.15
Mg-number	60.0	67.4	66.1	76.9	77.4	76.0	69.4	53.9	67.0	45.9	48.5	51.4
100Cr/(Cr+Al)	92.7	54.8	62.0	33.5	28.3	24.4	47.3	93.3	34.3	82.3	87.2	93.8

Continued on next page

Table 3 continued from previous page

Sample no:	WC251	LSC241	LSC240	LSC201	LSC 238	LSC 220	LSC 237	LSC 199	LSC 208	WC331	LSC204a	LSC204b
Lithology	C M W	C M W	C M L	C M W	C M W	C M W	C M W	C M P	C M P	C M P	C M P	C M P
SiO_2	0.15	0.16	0.20	0.18	0.19	0.22	0.21	0.13	0.13	0.13	0.20	0.19
TiO_2	0.58	0.59	0.56	0.59	1.39	0.53	1.42	1.13	2.54	1.54	3.92	1.56
Al_2O_3	9.29	6.58	5.86	6.37	7.14	6.69	6.32	6.45	3.57	8.77	2.42	3.37
Cr_2O_3	55.69	54.39	50.29	52.08	39.85	55.76	37.13	43.55	27.03	31.83	10.22	27.49
V_2O_3	0.12	0.15	0.13	0.16	0.22	0.10	0.28	0.15	0.30	0.30	0.49	0.25
FeO	22.63	27.26	32.32	30.64	41.86	25.59	46.28	40.56	57.63	47.83	73.97	58.83
MnO	0.33	0.35	0.40	0.44	0.52	0.37	0.45	0.49	0.49	0.44	0.25	0.39
MgO	10.48	8.14	7.26	8.29	5.52	8.94	4.80	5.47	3.51	5.47	2.51	3.01
NiO	0.14	0.09	0.20	0.10	0.13	0.10	0.16	0.13	0.20	0.15	0.11	0.11
ZnO	0.14	0.21	0.23	0.14	0.33	0.19	0.18	0.19	0.16	0.16	0.23	0.22
Total	99.60	97.95	97.47	99.03	97.20	98.51	97.29	98.27	95.62	96.68	94.43	95.46
Mg-number	52.5	42.3	38.7	43.0	29.8	46.3	25.9	29.2	19.6	29.1	14.2	16.9
100Cr/(Cr+Al)	80.1	84.7	85.2	84.6	78.9	84.8	79.8	81.9	83.6	70.9	73.9	84.6

Abbreviations: T = tectonite; C = cumulate; D = dunite; H = harzburgite; L = lherzolite; W = wehrlite; O = contains white orthopyroxene; M = mica; P = pyroxenite;

Table 4. Compositional data for orthopyroxenes from ultramafic xenoliths from the Bearpaw Mountains.

Sample no:	WC94	WC97	WC97	WC167	LSC263	WC171	WC297	WC297	WC251	LSC240	LSC197	LSC188
Lithology:	T H	T H	T H	T H	T L	T H	T H O	T H O	C M W	C M W	M Wb	M Wb
SiO_2	56.24	57.94	57.39	56.28	56.05	55.15	57.31	57.65	57.51	57.32	55.18	53.34
Al_2O_3	2.25	0.42	1.85	2.53	2.93	3.05	0.05	0.22	0.72	0.44	1.54	0.97
Cr_2O_3	0.39	0.26	0.39	0.39	0.39	0.57	<0.01	0.08	0.35	<0.01	0.18	0.08
FeO	5.36	5.29	5.42	5.55	5.91	5.63	7.24	7.17	5.71	8.70	14.81	23.55
MnO	0.15	0.14	0.14	0.12	0.12	0.16	0.16	0.27	0.13	0.23	0.34	0.31
MgO	34.42	34.58	34.17	34.07	34.01	33.40	34.14	33.26	34.42	33.02	28.53	22.04
CaO	0.47	0.98	0.32	0.40	0.40	0.85	<0.01	0.69	0.59	0.91	0.29	0.41
Na_2O	0.03	0.06	0.08	0.05	<0.02	0.06	0.03	0.05	0.05	<0.03	0.02	<0.01
Total	99.31	99.69	99.74	99.39	99.81	98.87	98.93	99.39	99.48	100.62	100.89	100.70
Mg=number	91.9	92.1	91.8	91.6	91.1	91.4	89.4	89.2	91.5	87.1	77.4	62.6

Abbreviations: T = tectonite; C = cumulate; H = harzburgite; L = lherzolite; W = wehrlite; O = contains white orthopyroxene; M = mica; Wb = websterite

Table 5. Compositional data for clinopyroxenes from ultramafic xenoliths from the Bearpaw Mountains.

Sample no:	WC97	WC167	LSC263	LSC260	WC235	WC251	LSC241	LSC240	LSC201
Lithology:	T H	T H	T L	T W	C M W	C M W	C M W	C M W	C M W
SiO_2	55.17	53.76	54.15	54.46	54.14	54.31	54.03	53.91	52.92
TiO_2	0.04	<0.01	<0.01	0.02	0.12	0.11	0.12	0.14	0.12
Al_2O_3	0.48	2.77	3.27	0.28	1.06	1.31	1.09	0.69	1.33
Cr_2O_3	0.98	0.85	0.92	0.89	0.97	1.24	0.97	0.71	0.11
FeO	2.28	2.40	1.92	2.06	2.95	2.31	3.16	2.93	4.80
MnO	0.10	0.06	0.10	0.10	0.12	0.10	0.13	0.09	0.16
MgO	18.02	16.89	16.47	17.82	17.38	17.24	17.83	17.20	16.16
CaO	22.25	22.34	23.09	22.96	22.35	21.84	22.15	23.47	22.51
Na_2O	0.58	0.61	0.90	0.54	0.51	0.97	0.53	0.28	0.50
Total	99.90	99.68	100.82	99.13	99.60	99.43	100.01	99.42	98.61
Mg-number	93.4	92.7	93.8	93.8	91.7	93.0	90.9	91.3	85.7

Sample no:	LSC 238	LSC 237	LSC 199	LSC 208	WC331	LSC204	LSC225	LSC197	LSC188
Lithology	C M W	C M W	C M P	C M P	C M P	C M P	C G	M Wb	M Wb
SiO_2	53.20	53.52	53.62	53.38	52.97	53.10	52.99	54.12	52.60
TiO_2	0.27	0.24	0.27	0.10	0.20	0.14	0.15	0.04	0.39
Al_2O_3	1.15	1.83	1.40	0.93	1.43	0.99	1.37	1.70	3.57
Cr_2O_3	0.31	0.13	0.56	0.15	0.11	0.08	0.05	0.37	0.22
FeO	5.45	6.79	4.84	5.90	5.65	6.49	5.54	3.87	8.17
MnO	0.17	0.23	0.12	0.22	0.18	0.27	0.19	0.14	0.16
MgO	16.02	15.70	16.23	15.96	15.61	15.67	15.11	15.92	13.03
CaO	22.59	22.46	23.28	22.33	22.57	22.11	22.98	23.36	21.07
Na_2O	0.35	0.47	0.31	0.46	0.43	0.40	0.69	0.60	1.20
Total	99.51	101.37	100.63	99.43	99.15	99.25	99.07	100.12	100.41
Mg-number	83.9	80.5	85.7	82.7	83.1	81.1	83.0	88.1	74.0

Abbreviations: T = tectonite; C = cumulate; H = harzburgite; L = lherzolite; W = wehrlite; M = mica; P = pyroxenite; Wb = websterite; G = Glimmerite

Table 6. Compositional data for phlogopites from ultramafic xenoliths from the Bearpaw Mountains.

Sample no:	LSC247	WC98	LSC260	WC296	WC297	WC253	WC232	WC251	LSC241	LSC240	LSC201
Lithology:	T D	T H	T W	T H O	T H O	C M W	C M D	C M W	C M W	C M L	C MW
SiO_2	40.64	37.69	39.27	39.53	40.65	39.28	40.70	39.17	39.79	40.17	39.64
TiO_2	0.65	0.26	0.40	0.70	1.58	1.08	0.58	0.92	0.60	0.78	1.29
Al_2O_3	12.21	16.38	13.51	15.12	12.50	14.08	12.46	14.05	14.00	13.82	13.52
Cr_2O_3	1.50	1.58	1.60	1.19	0.88	1.85	1.10	1.61	0.96	0.30	0.81
FeO	3.28	3.54	3.65	3.72	3.95	4.48	3.14	3.92	4.84	5.02	5.20
MnO	0.03	0.03	0.03	0.08	0.06	0.03	0.02	0.03	0.04	0.04	0.05
MgO	24.85	23.56	24.19	23.99	24.64	23.07	25.22	23.16	23.64	23.57	23.67
NiO	0.08	0.06	0.06	0.15	0.04	0.17	0.23	0.19	0.05	0.04	0.11
BaO	0.26	1.00	1.17	0.05	0.08	0.39	0.43	0.43	0.23	0.38	0.40
Na_2O	0.22	0.46	0.27	0.70	0.62	0.71	0.43	0.46	1.71	1.30	1.17
K_2O	10.33	9.27	9.70	9.18	9.22	8.91	9.73	9.45	7.62	8.23	8.60
F	0.39	1.05	0.41	1.45	1.26	0.32	1.65	1.37	0.17	0.24	0.30
Cl	0.01	0.07	0.01	0.12	0.09	0.05	0.03	0.04	0.02	0.03	0.02
Total	94.45	94.95	94.27	95.98	95.57	94.42	95.72	94.80	93.67	93.92	94.78
Mg-number	93.1	92.2	92.2	92.0	91.7	90.2	93.5	91.3	89.7	89.3	89.0

Continued on next page

Table 6 continued

Sample no:	LSC238	LSC220	LSC 237	LSC 199	LSC 208	WC331	LSC204	LSC225	LSC197	LSC188
Lithology	C M W	C M W	C M W	C M P	C M P	C M P	C M P	C G	M Wb	M Wb
SiO_2	38.42	40.16	37.87	37.62	38.79	37.99	38.26	38.86	39.62	38.74
TiO_2	1.52	0.77	1.82	2.28	1.57	2.17	1.69	1.30	0.88	4.35
Al_2O_3	14.51	13.13	14.49	14.46	13.91	14.61	13.70	14.06	14.24	12.56
Cr_2O_3	0.26	0.58	0.46	0.54	0.38	0.39	0.21	0.29	0.63	0.25
FeO	7.59	4.42	8.17	8.51	8.06	8.24	10.12	8.98	5.01	11.70
MnO	0.06	0.03	0.05	0.07	0.05	0.05	0.08	0.10	0.03	0.07
MgO	21.10	24.57	20.71	20.13	21.79	20.17	20.31	20.26	23.20	17.57
NiO	0.04	0.05	0.03	0.10	0.08	0.05	0.05	0.03	0.33	0.08
BaO	0.52	0.26	0.57	0.70	0.52	0.72	0.50	0.35	0.23	0.28
Na_2O	1.16	0.83	1.42	0.78	1.13	0.89	1.00	0.43	0.32	0.20
K_2O	8.32	8.89	7.99	8.94	8.31	8.79	8.61	9.61	9.78	9.68
F	0.19	0.28	0.23	0.33	0.20	0.36	0.25	0.35	1.93	1.53
Cl	0.04	0.02	0.03	0.03	0.03	0.04	0.03	0.03	0.03	0.33
Total	93.73	93.99	93.84	94.49	94.82	94.47	94.81	94.77	96.23	97.35
Mg-number	83.2	90.8	81.9	80.8	82.8	81.4	78.2	80.1	89.2	72.8

Abbreviations: T = tectonite; C = cumulate; D = dunite; H = harzburgite; L = lherzolite; W = wehrlite; O = contains white orthopyroxene; M = mica; P = pyroxenite; Wb = websterite; G = Glimmerite

Table 7. Temperature and fO_2 estimates from ultramafic xenoliths from the Bearpaw Mountains, using the method of Ballhaus et al. (1991).

	Lithology	T°C	$\Delta(fO_2)^{FMQ}$
Spinel peridotite tectonites			
LSC 247	Dunite	1089	0.87
WC 94	Harzburgite	950	0.83
WC 97	Harzburgite	971	0.57
LSC 260	Wehrlite	1038	0.91
WC 167	Harzburgite	1011	-0.19
LSC 263	Lherzolite	863	-1.10
WC 171	Harzburgite	945	0.14
Spinel peridotite tectonites with white orthopyroxene			
WC 297	Harzburgite	933	1.23
Mica peridotite cumulates			
WC 253	Mica wehrlite	937	0.34
WC251	Mica wehrlite	929	0.42
LSC241	Mica wehrlite	965	0.54
LSC240	Mica wehrlite	948	1.12
LSC201	Mica wehrlite	1011	0.93

Table 8. Whole-rock compositional data for spinel peridotite tectonite xenoliths from the Bearpaw Mountains.

Sample no:	LSC247	WC94	WC97	WC98	WC167	LSC263	LSC171	LSC260	WC296	WC297
Lithology:	T D	T H	T H	T H	T H	T L	T H	T W	T H O	T H O
SiO_2	38.75	40.90	40.86	41.59	41.91	45.96	41.61	40.27	40.35	38.34
TiO_2	0.044	0.012	0.016	0.022	0.017	0.013	0.015	0.029	0.049	0.026
Al_2O_3	0.29	0.76	0.83	1.10	1.20	1.79	1.04	0.21	1.26	0.82
Fe_2O_3	8.31	8.13	8.15	8.23	7.87	8.16	8.03	9.53	9.59	10.90
MnO	0.119	0.114	0.117	0.117	0.119	0.120	0.114	0.151	0.329	0.216
MgO	46.42	45.09	44.40	43.20	41.91	41.95	41.64	46.19	41.31	40.78
CaO	0.12	0.32	0.60	0.78	0.71	1.48	0.80	1.02	0.12	0.10
K_2O	0.119	0.010	0.145	0.038	0.004	0.005	0.008	0.083	0.202	0.140
P_2O_5	0.032	0.009	0.015	0.017	0.013	0.011	0.010	0.045	0.014	0.015
LOI	4.78	4.43	4.52	4.77	6.11	0.50	6.49	2.20	6.31	7.74
Total	98.96	99.77	99.70	99.87	99.88	100.01	99.75	99.76	99.52	99.10
Ba	34	3	361	66	8	<3	17	53	18	<3
Cr	4261	1974	1900	1872	2140	2854	1823	2520	2118	2349
Ni	2440	2415	2406	2289	2180	1908	2355	2259	2273	2450
Rb	8	<2	8	3	<2	<2	2	5	15	12
Sc	1	7	6	8	7	7	8	5	7	4
Sr	7	4	38	21	8	14	8	105	13	9
V	23	23	26	29	34	53	31	74	16	8
Zn	50	42	44	46	43	42	42	63	62	139
Zr	2	3	4	3	2	3	3	8	4	13

All values of Na_2O were below detection limit.

Abbreviations: T = tectonite; D = dunite; H = harzburgite; L = lherzolite; W = wehrlite;
O = contains white orthopyroxene; M = mica

Table 9. Whole-rock compositional data for mica peridotite cumulate xenoliths from the Bearpaw Mountains.

Sample no:	WC533	WC232	WC251	LSC241	LSC240	LSC201	LSC233	LSC232	LSC231	LSC 238	LSC 220	LSC 230
Lithology	C M W	C M D	C M W	C M W	C M L	C M W	C M D	C M L	C M L	C M W	C M W	C M W
SiO_2	39.43	39.08	39.23	42.91	43.52	43.17	43.41	43.08	42.89	42.56	44.80	43.43
TiO_2	0.105	0.072	0.109	0.227	0.305	0.375	0.270	0.276	0.527	0.670	0.302	0.650
Al_2O_3	1.55	1.06	1.64	4.81	5.02	3.92	4.87	4.53	5.54	6.80	5.66	6.85
Fe_2O_3	9.20	6.94	8.53	9.31	8.97	9.68	8.19	9.73	11.51	10.98	8.47	10.61
MnO	0.126	0.088	0.121	0.126	0.136	0.152	0.115	0.158	0.199	0.199	0.122	0.185
MgO	42.09	41.75	41.16	34.37	32.50	32.01	31.45	31.16	26.04	24.76	23.93	22.96
CaO	1.00	0.79	0.99	2.10	3.83	6.13	4.51	3.59	6.95	7.16	6.87	8.23
Na_2O	b.d.l.	b.d.l	b.d.l	0.75	0.48	0.39	0.47	0.67	0.55	0.60	0.57	0.60
K_2O	0.576	0.447	0.410	1.835	2.657	2.064	2.190	1.933	2.483	3.383	2.916	3.303
P_2O_5	0.045	0.053	0.066	0.078	0.313	0.157	0.110	0.248	0.323	0.505	0.060	0.411
LOI	5.47	9.20	7.22	3.00	1.83	1.48	3.55	3.75	1.94	1.53	5.45	1.69
Total	99.63	99.54	99.55	99.51	99.54	99.51	99.13	99.13	98.96	99.16	99.15	98.92
Mg-number												
Ba	193	204	150	669	1131	1097	823	726	1440	2037	801	2066
Cr	2649	2835	3416	2440	2570	2628	1722	2075	2136	1750	3554	1761
Ni	2363	2342	2285	1583	1668	1360	1550	1404	1117	1037	1995	873
Rb	27	23	18	87	102	98	110	98	127	147	171	145
Sc	4	5	5	8	11	14	18	10	14	17	10	20
Sr	35	37	36	181	258	157	256	287	321	216	189	231
V	32	15	36	57	80	106	85	79	129	188	102	181
Zn	66	41	60	67	77	75	54	79	104	101	63	98
Zr	11	5	8	17	27	15	26	43	28	21	14	20

Abbreviations: C = cumulate; D = dunite; L = lherzolite; W = wehrlite; M = mica;

Table 10. Whole-rock compositional data for mica clinopyroxenite and mica websterite xenoliths from the Bearpaw Mountains.

Sample no:	LSC 237	LSC 199	LSC26	LSC 208	WC331	LSC204	LSC225	LSC197	LSC188
Lithology	C M W	C M P	C MP	C M P	C M P	C M P	C G	M Wb	M Wb
SiO_2	43.26	41.31	42.90	43.03	43.63	43.02	41.97	48.93	46.00
TiO_2	0.559	0.790	0.787	0.637	0.680	0.860	0.986	0.314	1.951
Al_2O_3	4.70	6.06	4.93	6.09	5.04	7.48	11.57	6.09	6.57
Fe_2O_3	12.35	13.05	12.70	11.00	10.68	11.87	9.19	11.27	16.97
MnO	0.200	0.196	0.200	0.191	0.174	0.177	0.127	0.207	0.211
MgO	25.62	25.59	25.24	24.21	23.21	18.87	18.67	23.23	15.92
CaO	8.52	6.09	8.42	8.02	10.12	8.81	5.84	5.03	7.70
Na2O	0.46	0.39	0.32	0.62	0.41	0.74	0.50	0.27	0.66
K2O	1.956	3.177	2.257	2.885	2.132	4.036	7.038	2.887	2.627
P2O5	0.387	0.321	0.519	0.437	0.624	0.642	0.441	0.032	0.166
LOI	1.13	2.09	1.13	1.80	2.41	2.48	2.88	1.20	0.92
Total	99.13	99.06	99.40	98.93	99.11	98.99	99.21	99.46	99.70
Mg-number									
Ba	1656	2166	1709	1972	2045	n.a.	2595	483	777
Cr	1704	2193	1766	1784	1582	n.a.	2139	2381	1410
Ni	1027	1035	1037	968	828	n.a.	337	1269	974
Rb	93	149	93	121	104	n.a.	380	165	155
Sc	25	16	25	21	21	n.a.	11	18	26
Sr	203	153	231	182	276	n.a.	163	39	90
V	185	215	226	200	194	n.a.	208	104	263
Zn	98	120	110	89	85	n.a.	83	142	225
Zr	22	15	32	15	22	n.a.	23	31	89

Abbreviations: C = cumulate; W = wehrlite; M = mica; P = pyroxenite; Wb = websterite; G = glimmerite

Table 11 Trace element analyses of Bearpaw samples by solution ICP-MS

Spinel peridotite tectonites

	LSC 247	WC 94	WC 97	WC 98	WC 167	LSC 263	WC 171	LSC 260	WC 296	WC 297
ppm	T D	T H	T H	T H	T H	T L	T H	T W	T H O	T H O
Rb	5.5	0.7	7.5	2.4	0.8	0.4	1.1	4.2	15.9	10.6
Sr	6.8	3.9	41	21.4	9	13.1	7.2	105	13.2	7.3
Y	0.17	0.05	0.88	0.31	0.28	0.24	0.16	1.21	0.92	0.54
Zr	0.77	0.49	1.98	0.77	0.24	1.05	0.61	5.2	1.01	12
Nb	0.1	0.05	0.76	0.21	0.05	0.07	0.18	0.34	0.5	1.02
Cs	0.13	0.11	0.62	0.2	0.09	0.02	0.22	0.11	1.75	0.99
Ba	27.7	2.1	387	56	2.7	3.7	4.4	53	18.6	5.9
La	0.25	0.36	1.47	0.8	0.54	0.66	0.23	2.15	0.24	1.17
Ce	0.5	0.51	3.12	1.71	1.19	1.3	0.43	4.68	0.47	2.04
Pr	0.06	0.04	0.4	0.22	0.15	0.13	0.05	0.59	0.05	0.2
Nd	0.28	0.11	1.69	0.89	0.61	0.49	0.17	2.45	0.2	0.68
Sm	0.06	0.02	0.35	0.14	0.1	0.06	0.03	0.51	0.05	0.12
Eu	0.02	0.01	0.08	0.04	0.02	0.02	0.01	0.14	0.01	0.02
Gd	0.06	0.01	0.28	0.09	0.07	0.04	0.02	0.4	0.07	0.09
Tb	0.007	0.001	0.03	0.01	0.007	0.005	0.036	0.05	0.016	0.14
Dy	0.04	0.01	0.19	0.06	0.05	0.03	0.03	0.27	0.14	0.1
Ho	0.007	0.002	0.031	0.011	0.01	0.009	0.006	0.045	0.034	0.021
Er	0.02	0.01	0.09	0.04	0.03	0.03	0.02	0.12	0.11	0.07
Tm	0.003	0.002	0.014	0.006	0.006	0.007	0.004	0.018	0.019	0.013
Yb	0.02	0.02	0.09	0.05	0.04	0.05	0.03	0.13	0.14	0.1
Lu	0.005	0.004	0.018	0.01	0.008	0.012	0.007	0.025	0.025	0.02
Hf	0.02	0.01	0.06	0.02	0.01	0.02	0.02	0.14	0.03	0.31
Ta	0.005	0.002	0.033	0.008	0.003	0.002	0.004	0.022	0.041	0.052
Pb	0.17	0.31	0.59	0.42	0.23	0.28	0.35	0.41	1.72	2.1
Th	0.08	0.09	0.81	0.14	0.17	0.06	0.07	0.92	0.11	1.01
U	0.62	0.17	0.44	2.49	0.13	0.85	0.08	15.7	0.48	0.78
(La/Yb)n	8.36	12.04	10.92	10.7	9.03	8.83	5.13	11.06	1.14	7.83
Eu/Eu*	0.91	1.18	0.84	0.98	0.91	1.11	1.01	0.94	0.57	0.53

Table 11 continued

Mica peridotite cumulates

	WC 253	WC 251	LSC 241	LSC 241	LSC 240	LSC 201	LSC 233	LSC 232	LSC 231	LSC 238	LSC 220	LSC 230
ppm	C M W	C M W	C M W	repeat	C M L	C M W	C M D	C M L	C M L	C M W	C M W	C M W
Rb	26.6	18.7	83	82	103	92	115	94	122	140	162	133
Sr	34.3	38	182	178	282	163	288	292	324	217	192	231
Y	1.52	2.23	2.97	2.9	7	4.31	2.77	5.7	7.6	12.8	1.97	9.6
Zr	8.5	6.8	14.9	14.7	23.6	11.7	24.4	37.6	22.4	15.7	10.2	14.6
Nb	0.51	0.66	1.71	1.74	3.18	1.67	2.2	2.86	3.75	5.9	0.98	3.89
Cs	1.47	0.82	3.06	3.03	3.61	2.48	4.12	4.01	3.69	4.16	4.4	4.21
Ba	229	159	667	679	1058	881	788	713	1315	1834	775	1801
La	1.44	1.96	3.15	3.27	11.1	4.47	4.22	9	10.7	14.4	2.51	10.7
Ce	3.01	4.34	6.8	7.1	22.7	10	7.8	18.4	23.1	34	4.84	23.8
Pr	0.39	0.56	0.89	0.91	2.68	1.34	0.88	2.21	2.93	4.35	0.61	3.19
Nd	1.71	2.75	4.29	4.24	11.9	6.4	3.84	9.5	13.4	19.7	2.82	15.3
Sm	0.41	0.68	0.94	0.97	2.48	1.51	0.87	1.95	2.79	4.26	0.69	3.37
Eu	0.11	0.22	0.29	0.29	0.65	0.4	0.23	0.56	0.79	1.11	0.2	0.91
Gd	0.39	0.66	0.89	0.92	2.09	1.36	0.82	1.71	2.52	3.96	0.71	3.19
Tb	0.051	0.084	0.107	0.111	0.256	0.17	0.099	0.218	0.301	0.485	0.084	0.379
Dy	0.32	0.51	0.63	0.66	1.49	1	0.58	1.24	1.75	2.88	0.47	2.26
Ho	0.06	0.089	0.115	0.121	0.272	0.176	0.107	0.232	0.312	0.51	0.08	0.404
Er	0.17	0.25	0.32	0.34	0.72	0.46	0.3	0.65	0.81	1.39	0.24	1.08
Tm	0.025	0.033	0.044	0.045	0.099	0.065	0.043	0.09	0.11	0.18	0.03	0.143
Yb	0.17	0.2	0.27	0.29	0.62	0.39	0.26	0.57	0.69	1.13	0.19	0.86
Lu	0.03	0.034	0.046	0.046	0.101	0.062	0.044	0.095	0.114	0.181	0.034	0.136
Hf	0.25	0.24	0.47	0.49	0.72	0.4	0.62	1.11	0.74	0.61	0.27	0.57
Ta	0.028	0.033	0.079	0.084	0.143	0.075	0.099	0.15	0.168	0.254	0.049	0.164
Pb	2.38	1.6	4.39	4.48	2.4	1.22	4.62	1.51	3.09	1.61	1.52	1.55
Th	0.58	0.71	0.83	0.89	3.47	0.71	2.25	3	1.41	0.92	1	0.78
U	4.82	2.79	1.03	1.07	1.35	0.279	1.78	1.53	0.63	0.71	1.45	0.337
(La/Yb)n	5.67	6.55	7.81	7.54	11.97	7.66	10.86	10.56	10.37	8.52	8.84	8.32
Eu/Eu*	0.86	0.99	0.96	0.94	0.88	0.86	0.85	0.94	0.92	0.83	0.86	0.85

Table 11 continued

	Mica clinoproxenite cumulates							Mica websterites		Standard
	LSC237	**LSC199**	**LSC26**	**LSC208**	**WC331**	**LSC225**		**LSC197**	**LSC188**	**UBN**
ppm	C M P	C M P	C M P	C M P	C M P	C G		M Wb	M Wb	
Rb	89	151.6	88.60	132.2	96.00	397.2		160.8	146.5	3.5
Sr	209	148.7	234.1	181.5	277.0	166.5		37.60	89.50	8.5
Y	9.6	7.41	15.28	10.76	10.75	7.06		9.60	19.35	2.57
Zr	18.6	10.60	28.76	10.57	16.76	18.36		6.57	35.88	3.67
Nb	2.17	4.54	4.36	3.03	3.17	3.99		3.98	24.12	0.1
Cs	2.5	3.00	2.51	3.92	2.52	7.59		3.42	3.34	11.97
Ba	1350	1814	1447	1804	1747	2349		369.9	634.2	29.36
La	7.9	6.99	12.90	9.56	14.67	11.03		1.66	17.48	0.44
Ce	19.1	16.64	30.03	22.32	34.11	23.50		6.21	47.75	1
Pr	2.6	2.27	4.09	3.06	4.59	2.89		0.99	6.61	0.13
Nd	12.7	10.83	19.68	14.74	21.56	12.60		4.94	30.50	0.7
Sm	2.9	2.34	4.38	3.32	4.37	2.49		1.32	6.28	0.23
Eu	0.83	0.64	1.23	0.91	1.22	0.67		0.13	1.33	0.09
Gd	2.86	2.34	4.27	3.35	3.87	2.38		1.60	5.70	0.34
Tb	0.35	0.28	0.54	0.42	0.44	0.27		0.25	0.75	0.06
Dy	2.01	1.60	3.16	2.45	2.42	1.54		1.73	4.35	0.48
Ho	0.36	0.29	0.57	0.45	0.42	0.28		0.35	0.75	0.1
Er	0.9	0.72	1.47	1.14	1.04	0.72		0.96	1.86	0.3
Tm	0.12	0.10	0.20	0.15	0.14	0.10		0.14	0.25	0.05
Yb	0.72	0.58	1.21	0.89	0.78	0.59		0.88	1.46	0.31
Lu	0.115	0.09	0.19	0.14	0.12	0.10		0.14	0.22	0.05
Hf	0.63	0.39	1.05	0.43	0.62	0.62		0.33	1.63	0.14
Ta	0.111	0.20	0.20	0.13	0.15	0.19		0.27	1.55	0.02
Pb	2.1	1.61	3.07	1.25	1.65	4.76		1.19	4.24	13.85
Th	0.95	0.36	1.37	0.41	0.89	1.02		0.20	1.07	0.09
U	0.332	0.52	0.84	0.78	0.49	0.35		0.13	0.43	0.07
(La/Yb)n	7.34	8.06	7.13	7.18	12.58	12.5	1.26	1.26	8.01	
Eu/Eu*	0.88	0.84	0.87	0.84	0.91	0.85		0.27	0.68	

Table 12. Trace element (in ppm) and isotopic data for clinopyroxenes and phlogopite from ultramafic xenoliths from the Bearpaw Mountains.

Sample no.	LSC263	LSC260	LSC260	LSC201	LSC237	LSC188
Lithology	T L	T W Core	TW rim	C M W	C M P	M Wb
ppm						
La	10.43	12.5	12.8	2.5	4.05	13.25
Ce	21.00	25.9	26.7	8.25	14.3	43.05
Pr	2.20	3.0	3.1	1.5	2.46	6.45
Nd	6.97	9.45	10.3	7.79	10.9	27.4
Sm	0.87	1.35	1.45	2.36	3.61	6.30
Eu	0.24	0.36	0.36	0.69	1.14	1.45
Gd	0.62	0.9	1.0	2.13	3.17	5.25
Tb	0.07	0.13	0.13	0.29	0.47	0.75
Dy	0.39	0.7	0.7	1.64	2.70	3.89
Ho	0.08	0.14	0.14	0.29	0.48	0.70
Er	0.35	0.6	0.5	0.68	1.27	1.75
Yb	0.47	0.7	0.7	0.60	1.17	1.2
Lu	0.08	0.09	0.09	0.09	0.16	0.16
Ba	0.47	445.7	88.5	6.8	6.69	2.65
Rb	0.20	19.2	1.1	0.81	1.46	0.40
Sr	117.3	286.1	270.5	173.9	240.4	20.2
Nb	0.19	1.0	0.51	0.04	0.09	0.29
Ta	0.01	0.08	0.029	0.006	0.008	0.11
Zr	0.17	9.8	8.3	8.4	16.5	45.6
Hf	0.01	0.17	0.15	0.35	0.69	2.63
Y	2.50	4.4	4.0	7.3	12.4	15.6
Pb	1.10	1.7	1.5	0.59	1.05	2.6
U	0.06	1.9	0.9	0.04	0.07	0.10
Th	0.25	0.8	0.6	0.12	0.21	0.37
$^{87}Sr/^{86}Sr_m$	0.70468±1	0.70639±1	-	0.70715±1	0.70714±1	0.74844±1
$^{143}Nd/^{144}Nd_m$	0.510741±4	0.512109±5	-	0.512084±4	0.512037±4	0.511263±4
εNd	-37.1	-10.3		-10.8	-11.8	-26.9

LSC188 (phlogopite) $^{87}Sr/^{86}Sr_m$ = 1.191752±15; Rb = 404.2 ppm; Sr = 44.5 ppm; $^{87}Rb/^{86}Sr$ = 27.4265

Abbreviations: T = tectonite; C = cumulate; W = wehrlite; M = mica; P = pyroxenite; Wb = websterite.